A STUDY OF CONFORMAL PHASES IN METAL ALLOY SYSTEMS

Thesis by

Paul Pietrokowsky

In Partial Fulfillment of the Requirements

For the Degree of

Doctor of Philosophy

California Institute of Technology

Pasadena, California

1959

ACKNOWLEDGMENT

The author wishes to express his gratitude to Professor Pol Duwez for the interest he has shown in this research. It is a pleasure to acknowledge the beautiful X-ray photographs made with the Hägg designed Guinier type camera, through the efforts of Dr. Sten Sampson and Dr. Georg Lundgren. The painstaking metallography was performed by Mrs. V. Johnson. The author received assistance in alloy preparation and heat treatment from Mr. E. Frink, and in addition owes Mr. F. Youngkin an expression of gratitude for his contributions to the cylindrical camera which was used in a spectrometer geometry.

ABSTRACT

The atomic motifs of the intermediate phases $TiAu_4$ and $TiPt_8$ have been investigated. Both crystal structures are tetragonal. Lattice parameters of $TiAu_4$, 80 atomic percent gold, are $a_2 = b_2 = 6.460(5)$ Å and $c_2 = 3.976(5)$ Å. There are ten atoms in the unit cell; two titanium atoms were placed in positions (a) and eight gold atoms were placed in (h) of space group C_{4h}^5 - I4/m. The positional parameters were determined to be $x = 0.200 \pm 0.001$ and $y = 0.3970 \pm 0.0008$. Lattice parameters of $TiPt_8$ are $a_3 = b_3 = 8.312$ Å and $c_3 = 3.897$ Å. The unit cell contains eighteen atoms. Space group D_{4h}^{17}-I4/mmm was used: the two titanium atoms were placed in (a), eight gold atoms in (h) with parameter x_1, and eight gold atoms in (i) with parameter x_2. The positional parameters were determined to be $x_1 = 0.333$ and $x_2 = 0.327$. The use of conformal transformations in these investigations is discussed.

A result of this investigation has been the redetermination of the partial constitution diagram $TiAu_2$-Au. Two intermediate phases were established. The phase $TiAu_2$ is congruent melting. It is tetragonal with lattice parameters $a = b = 3.4192$ Å and $c = 8.513$ Å. The crystal structure has been determined. The two titanium atoms are in (a), of space group D_{4h}^{17}-I4/mmm, and the four gold atoms are in (e) with $z = 0.337$. A second intermediate phase, $TiAu_4$, displays a

hidden maximum. The solubility limit of titanium in gold has been studied as a function of temperature. In addition, the region of homogeneity of $TiAu_4$ has been investigated.

The alloys TiFe, TiCo, and TiNi have been investigated by X-ray diffraction methods. Evidence for long-range order in these phases has been established. Thus these alloys are of the CsCl type crystal structure type.

TABLE OF CONTENTS

PART		PAGE
INTRODUCTION		1
I.	AN INVESTIGATION OF THE SOLID STATE PHYSICAL METALLURGY OF TITANIUM-GOLD ALLOYS IN THE PARTIAL PHASE DIAGRAM $TiAu_2$-Au	4
	Introduction	5
	Metallography of the partial constitution diagram $TiAu_2$-Au	8
	X-Ray diffraction results	16
	Discussion	39
II.	LONG-RANGE ORDER IN TiFe, TiCo, and TiNi	53
	Introduction	54
	Discussion	55
	The diffraction experiment	62
	Results	67
III.	THE CONFORMAL PHASE $TiPt_8$	72
	Introduction	73
	The intensity expression	77
	The crystal structure of $TiPt_8$	84
	Discussion	92
CONCLUSIONS		95
MATERIALS		98
EXPERIMENTAL PROCEDURES		98
REFERENCES		101

INTRODUCTION

Since physical metallurgy is an applied science one might expect the technological interest in a given metal to be related to its abundance. Clarke and Washington (1) have estimated the average composition of elements existing in the upper ten miles of the earth's crust. From these results we observe that iron is the most plentiful transition element, third in the list of all naturally occurring elements. The next transition element to be found in this sequence is titanium, which is ninth in this tabulation. Our interest in iron and its alloys does indeed date from antiquity; yet titanium and titanium alloys have received intensive research in the laboratory only in the past ten years. Thus while both elements, iron as well as titanium, exist in nature as oxides our lack of knowledge of the latter metal is testimonial to the difficulty which has been encountered in its reduction from ore.

This thesis is an experimental investigation of several research problems, pertaining to the solid state physical metallurgy of titanium alloys, which originated during the recent period of accelerated activity. The relationship of the experiments of this thesis to the entire field of activity is complex, as one might surmise, and therefore the motivations for selecting the particular problems to be described are difficult to understand out of context. The wisdom of presenting all

the references on this subject is doubtful; even if this were done the reasoning which led to a closer examination of experiments reported in the literature might well become submerged in a sea of data. For this reason each investigation to be described herein shall be developed in terms of its immediate environment.

It may be useful, however, to make a few pertinent comments so as to place in proper perspective the value of our recently acquired understanding of titanium. Although basic research constituted only a small portion of the enormous effort which was expended, the physical metallurgist may derive some satisfaction from the fact that the importance of understanding constitution diagrams was realized and this work was performed simultaneously with the usual pedestrian activities which one associates with a materials development program. This modest effort to study the properties of titanium alloys has indeed been rewarding; this might have been foreseen, to some extent, from the nature of the metal itself. Titanium has the largest atomic radius of all transition elements residing in the first long period. In addition it exhibits allotropy in crystal structure which is unique amongst its neighbors in this period of the periodic table: transforming from body-centered cubic to the hexagonal close-packed low temperature modification. A wealth of information has been obtained on the relationship between atomic radii and solid solution alloying. This in turn does reflect in our confidence

and understanding of such observations as the Hume-Rothery rules (2). In addition to the equilibrium phase diagrams we have obtained a better understanding of some non-equilibrium processes in the solid state. Some research and thought has been devoted to the martensite transformation and the decomposition product, or products, which is described in the literature as the omega phase. Crystal structure determinations of many titanium alloys have yielded evidence for new types of atomic motifs as well as provided additional data on existing isomorphous structures such as the Laves phases and so called "beta-tungsten" type phase. The frequency which one finds the latter in titanium alloys is important since a member of this crystalline species, Nb_3Sn, is known to exhibit the highest transition temperature for superconductivity (3). Finally let us mention a subject which bears directly on the research of this thesis and represents one of the most aesthetically pleasing subjects in physical metallurgy. This is the modes of decomposition of a face-centered cubic solid solution into ordered phases.

PART I

AN INVESTIGATION OF THE SOLID STATE PHYSICAL METALLURGY OF TITANIUM-GOLD ALLOYS IN THE PARTIAL PHASE DIAGRAM $TiAu_2$-Au

INTRODUCTION

In an early investigation Wallbaum (4) reported the existence of a gold-rich phase having the stoichiometric composition $TiAu_3$. The crystal structure of this alloy was determined to be the ordered $AuCu_3$ or Ll_o type. An extensive study of alloys in the composition interval TiAu-Au was made by Raub, Walter, and Engel (5) whose results led to the partial constitution diagram which is displayed in figure 1. The latter investigators employed thermal analysis, metallographic, and X-ray methods. They were not able to confirm the occurrence of $TiAu_3$.

The experimental results of Raub et al. are interesting in several respects. First it was noted that the addition of titanium to gold solid solutions decreased the lattice parameter of the terminal phase, an effect which is opposite to that which one would normally expect on the basis of Vegard's law. Furthermore, an intermediate phase was reported, $TiAu_6$, of face-centered tetragonal lattice and four atoms per unit cell. The authors had deduced from X-ray diffraction evidence that this phase did exist over a very narrow composition interval. A similitude in the atomic motifs of the gold-rich alpha solid solutions and the intermediate phase $TiAu_6$ is evidenced by the reported axial ratio for the latter, approximately 0.97. The question of ordering in $TiAu_6$ was not discussed in the previous reference although under the circumstances one must assume some disorder to exist even though it might involve only one set of

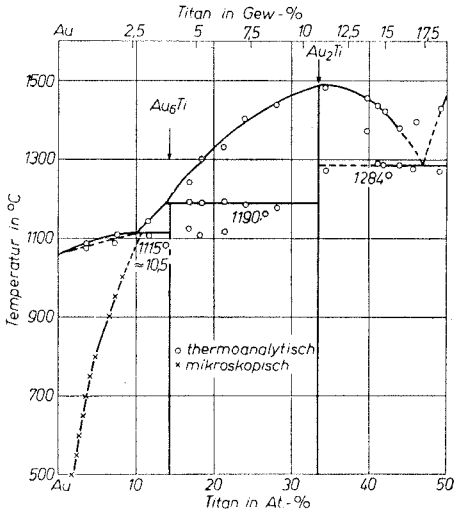

FIG. I. THE PARTIAL PHASE DIAGRAM TiAu-Au. AFTER RAUB et al (REFERENCE 5).

crystallographically equivalent sites. It is indeed curious that a phase such as $TiAu_6$ would exist over a narrow range of homogeneity when it is in fact disordered, complete long-range order only being possible at the composition which corresponds to $TiAu_3$. One might suspect, from the similarity in atomic arrangements of these gold-rich phases, that $TiAu_6$ could be a metastable phase similar to that which has been found in the kinetics of the ternary system Cu-Ni-Co by Geisler and Newkirk (6).

An attempt was made by the present author to confirm the crystal structure of $TiAu_6$ as deduced by Raub and coworkers. The investigation which was conducted failed to produce evidence for $TiAu_6$ but did yield data for a new intermediate phase, $TiAu_4$, which was related to the alpha solid solutions in a most interesting manner. The subsequent determination of the crystal structure of $TiAu_4$ made it very apparent that a serious attempt to find $TiAu_6$ would necessitate a re-determination of the partial phase diagram $TiAu_2$-Au. This was in fact accomplished.

METALLOGRAPHY OF THE PARTIAL CONSTITUTION DIAGRAM $TiAu_2$-Au

The various alloys which were prepared by electric arc melting displayed several characteristic microstructures when examined in the as-cast condition. From these observations it was possible to deduce, in a qualitative manner, the reactions which had taken place in the alloys during the process of solidification from the melt. Titanium-rich mixtures, $66\frac{2}{3}$ to 84 atomic percent gold, gave evidence that solidification had involved primary crystals of $TiAu_2$, peritectic $TiAu_4$ and gold solid solutions. The intermediate phase $TiAu_2$ was easily identified with polarized light since it showed a color change from violet to grey as a consequence of the anisotropy in lattice symmetry (figure 2). It was observed that $TiAu_2$ did react more readily with the aqua regia etchant than either of the gold-rich phases. In figure 3 we see the same alloy as in the previous photomicrograph (fig. 2) but here the $TiAu_2$ phase has been overetched. This is necessary to bring up the characteristic striations which we shall identify with $TiAu_4$. At this higher magnification we see very clearly that coring does exist in the terminal phase which is a continuous series of solid solutions. It is this observation which leads one to the conclusion that region of alpha plus melt in the phase diagram must exist over an appreciable temperature interval. Figure 4 is representative of ingots containing 86 and 88 atomic percent gold, in

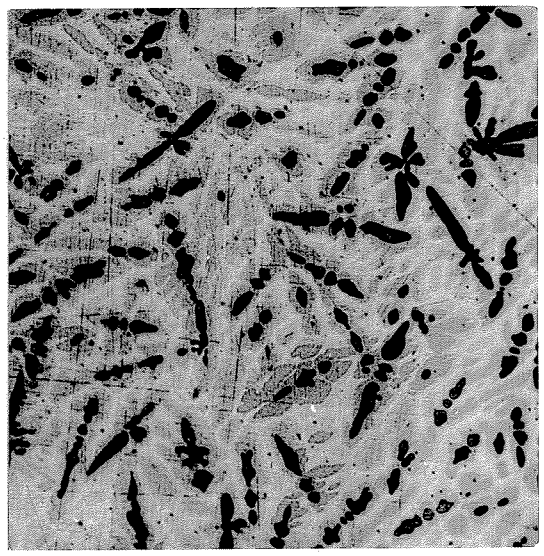

Fig. 2.--82 Atomic Pct Au. As cast. Etched lightly. 250X.

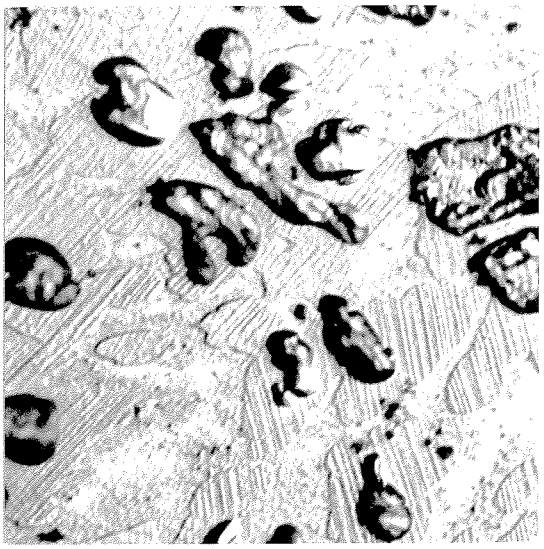

Fig. 3.--82 Atomic Pct Au. As Cast. Etched deeply. 1000X.

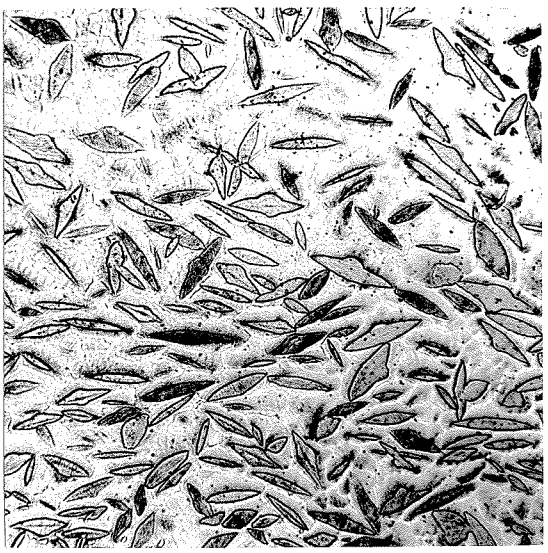

Fig. 4.--88 Atomic Pct Au. As cast. Etched. 150X.

Fig. 5.--91.9 Atomic Pct Au. Heat-treated at 1000°C for 30 minutes and water quenched. Etched. 250X.

which primary crystals of $TiAu_4$ were observed. The residual liquid solidified as gold solid solutions in which coring is evident. Alloys which contained more than 88 atomic percent gold showed heterogeneous grains of cored solid solutions of the terminal phase.

Those alloys which were ductile were deformed in a rolling mill so as to promote diffusion in subsequent heat treatment. A chemical analysis of these alloys is presented in Table I. All ingots were homogenized at 1000°C for 48 hrs prior to the equilibration heat-treatments which are described in Table II. In all cases, annealing was terminated by a water quench of the specimen from temperature.

A considerable region of continuous solid solutions of titanium in gold was observed. Figure 5 shows one such alloy in the alpha phase field. The dark spots which appear in the equiaxed alpha grains are etch pits (see figure 6); small amounts of $TiAu_4$ in alpha are easily delineated by various methods. For example, in a plane polished surface of such an alloy the $TiAu_4$ and alpha phases have different optical properties and we observe a different color for each phase. Etching such a specimen yields another method of identification (figure 3) as does the characteristic Widmanstätten pattern which results from the marked temperature dependence of solubility of the alpha phase. One must take exception to the previous statement for the low temperature heat-treatment (370 and 400°C) which results in a fine dispersion of $TiAu_4$

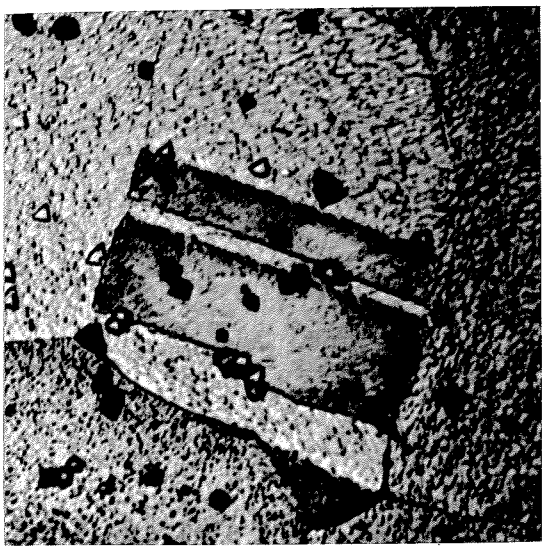

Fig. 6.--91.9 Atomic Pct Au. Heat-treated at 1000°C for 30 minutes and water quenched. Etched. 1000X.

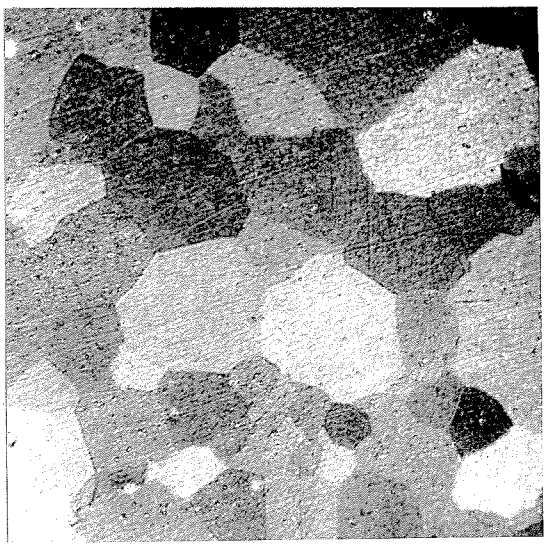

Fig. 7.--96.2 Atomic Pct Au. Heat-treated at 400°C for 30 days. Etched. 250X.

particles in the equiaxed grains of alpha (figure 7) which are darkened considerably by this general precipitation. Results of the metallography reveal that the solubility of titanium in gold is very temperature dependent (figure 8).

The only intermediate equilibrium phase observed to exist between $TiAu_2$ and the terminal alpha solid solutions was $TiAu_4$. An alloy containing 82 atomic percent gold was found to have a single phase microstructure and the 80 atomic percent gold alloy was almost single phase (figure 9), a small amount of $TiAu_2$ being present. The $TiAu_2$ is overetched and appears as voids in figure 9. X-Ray evidence demonstrates conclusively that the $TiAu_4$ phase field does indeed exist over a range of homogeneity and that both the 80 and 82 atomic percent alloys must exist in this region. This evidence will be presented later in the text. It will suffice, for the present, to say that the time of heat-treatment at 1000°C was not adequate to promote equilibrium in the peritectic reaction which is responsible for the formation of $TiAu_4$. One must realize that the investigation is being performed with very small specimens and that we seek to avoid excessive losses of alloying element due to vaporization. Preliminary experiments demonstrated that the times used for the heat-treatments, with exception of the lowest temperatures, were adequate to produce a consistent sequence of microstructures for the alpha solid solutions and two phase region which are in juxtaposition.

Optical metallography was found to be useful for incipient

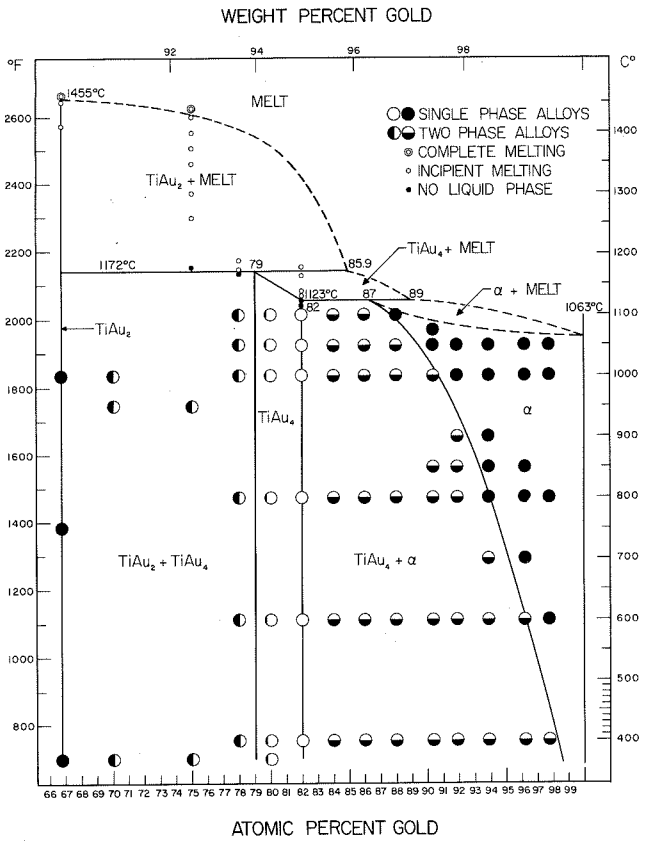

FIG. 8. THE PARTIAL CONSTITUTION DIAGRAM $TiAu_2$-Au. RESULTS OF THIS INVESTIGATION.

melting observations and consequently for determination of the peritectic temperatures. An alloy containing 82 atomic percent gold, which had been equilibrated in a single phase region, is shown in figure 10 after heat-treatment at 1140°C. The polyhedral grains which are characteristic of $TiAu_4$ (fig. 9) have now become rounded and in addition the alpha phase appears as a result of the solidification of the residual melt which was present at temperature. In the absence of alpha the $TiAu_4$ grains were always equiaxed; and from these observations the peritectic temperature for the reaction: $TiAu_4$ (82 atomic percent gold) + melt (89 atomic percent gold) $\rightleftarrows$ alpha solid solution (87 atomic percent gold) was determined to be 1123 ± 3°C. For the reaction: $TiAu_2$ ($66\frac{2}{3}$ atomic percent gold) + melt (85.9 atomic percent gold) $\rightleftarrows$ $TiAu_4$ (79 atomic percent gold), the peritectic temperature was established as 1172 ± 5°C. An alloy containing 82 atomic percent gold which had heated above this temperature is shown in figure 11. The microconstituents which are present after light etching are $TiAu_2$, $TiAu_4$, and alpha as is to be expected. The composition of the melt in this peritectic reaction has been selected to agree with the observations that the ingot containing 86 atomic percent gold solidified from the melt through a region of primary $TiAu_4$ and secondly that an alloy containing 85.7 atomic percent gold displayed some $TiAu_2$ in its microstructure when heated above 1172°C (see figure 11 for example).

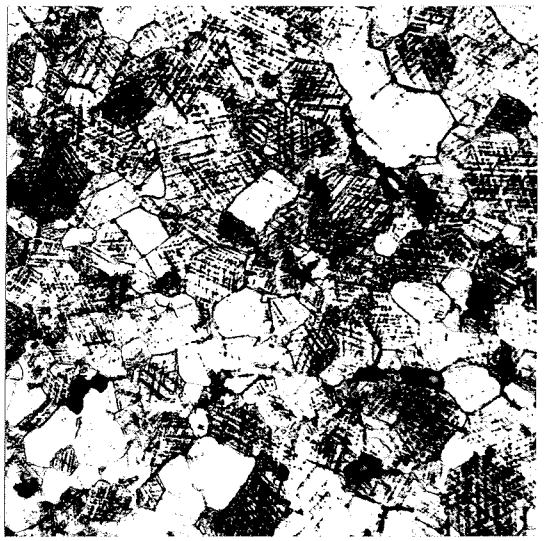

Fig. 9.--80 Atomic Pct Au. Heat-treated at 1000°C for 48 hours. Water quenched. Etched. 500X.

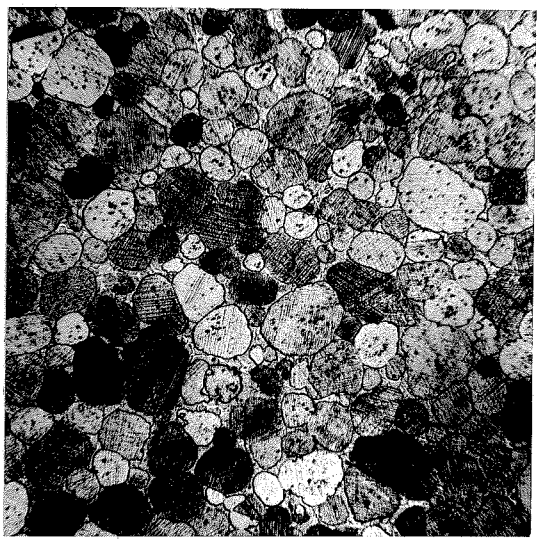

Fig. 10.--82 Atomic Pct Au. Heat-treated at 1140°C for 30 minutes. Water quenched. Etched. Side lighting. 1000X.

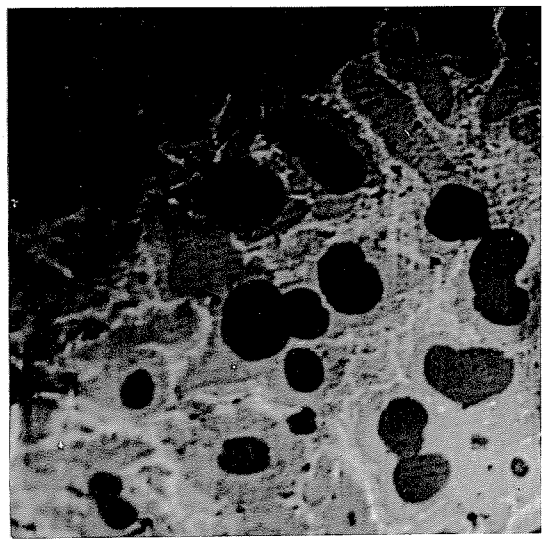

Fig. 11.--82 Atomic Pct Au. Heat-treated at 1177°C for 15 minutes. Water quenched. Etched lightly. 250X.

X-RAY DIFFRACTION RESULTS

Lattice Parameters of the Alpha Solid Solutions

The temperature dependence of the solubility limit of titanium in face-centered cubic gold was determined by metallography, figure 8. Debye-Scherrer X-ray powder photographs, of specimens quenched from the isothermal temperature into liquid argon, were used to study the variation of lattice parameter with alloying element. The magnitude of the cubic unit cell translations was determined by methods due to Cohen (7,8) or Nelson and Riley (9). These results are presented in Table III. It is estimated that the accuracy of these measurements is about 1 part in 20,000. Thus it would seem that both methods of extrapolation yield the same results under the conditions of the experiments. One might expect the data taken from films made with cobalt radiation to yield a more reliable result since this wavelength places five diffraction maxima, (420) $K\alpha_1 K\alpha_2$, (422) $K\beta$, and (331) $K\alpha_1 K\alpha_2$ in a region of back reflection which is sensitive to small variations in interplanar spacing. It was observed that the mean values of the lattice parameters was not influenced by the radiation which was used and for this reason these data, at each composition of interest, were averaged and plotted as a function of composition in figure 12. These results are in agreement with the observation of Raub, Walter, and Engel: the addition of

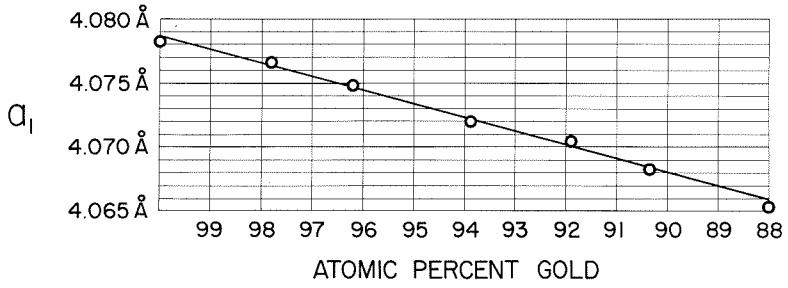

FIG. 12. LATTICE PARAMETER MEASUREMENTS OF THE GOLD-RICH ALPHA SOLID SOLUTIONS AS A FUNCTION OF COMPOSITION IN THE INTERVAL 88-98 ATOMIC PERCENT GOLD.

titanium to face-centered gold contracts the lattice parameter of the parent phase even though the atomic radii, for coordination number 12, of the solute atom is larger than that of the solvent atom. The present investigation, however, has demonstrated the existence of a more extensive region of alpha solid solubility than previously reported. It was not possible to utilize the lattice parameter versus composition data as a calibration curve for obtaining the solubility limit as is frequently done. This is because the alpha and $TiAu_4$ powder diffraction patterns overlap.

Lattice Parameters of the Intermediate Phase $TiAu_4$

The region of homogeneity for this intermediate phase was determined by X-ray powder diffraction methods. A 143.2 mm diameter Debye-Scherrer camera was used. Alloys which were investigated for this purpose are identified in Table IV with the extrapolated values of the lattice parameters as determined by Cohen's method. Cobalt radiation was used because this wavelength placed four well resolved Kα doublets in the back reflection region: (361), (433), (550), and (622) $K\alpha_{12}$. These spectra were used in least squares adjustment of the data and received equal weight in the equations of observations. The magnitudes of the unit cell translations, a_2 and c_2, are presented in figure 13 as a function of composition. The data points in this figure represent averaged lattice parameter values since it was observed that annealing temperature was

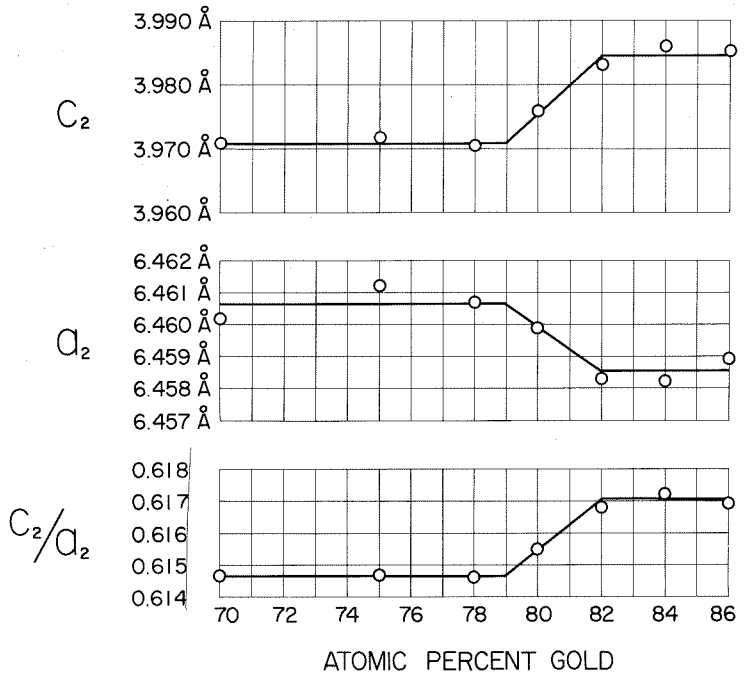

FIG. 13. LATTICE PARAMETER MEASUREMENTS AND AXIAL RATIO OF THE INTERMEDIATE PHASE $TiAu_4$ AS A FUNCTION OF COMPOSITION IN THE INTERVAL 70-86 ATOMIC PERCENT GOLD.

not a variable for a given composition. The results of these data indicate that $TiAu_4$ exists over a region of homogeneity from 79 to 82 atomic percent gold which is independent of temperature up to the liquidus. The addition of titanium to the gold-rich $TiAu_4$ decreases the atomic volume within the region of homogeneity of this intermediate phase. Thus, as was the case for the alpha solid solutions, titanium behaves as though its atomic radius was smaller than that of gold. This is not the case for these metals when in the elemental state, when their atomic radii have been corrected to the same coordination number. A word of caution must be expressed concerning the reliability of lattice parameters of the 84 atomic percent alloy. This alloy was a mixture of $TiAu_4$ and alpha and it was necessary to omit several back reflection lines of $TiAu_4$ from the least squares analyses because of superposition with diffraction maxima of alpha. No difficulty of this nature was encountered in two phase mixtures of $TiAu_2$ and $TiAu_4$.

The Crystal Structure of the Intermediate Phase $TiAu_2$

The crystal structure of this congruent melting phase has received attention in the literature only in that its lattice has been described as hexagonal close-packed (5). Were this the case one would expect primary crystals of $TiAu_2$ to exhibit hexagonal symmetry in the microstructure of alloys which had solidified through two phase regions of $TiAu_2$ plus melt. In

the present investigation it was observed that the cooling rate during solidification was too rapid to allow the growth of well defined crystals and for this reason it was difficult to establish crystal symmetry from the crystal morphology with complete confidence. Examination of many primary crystals of $TiAu_2$ indicated the presence of a four-fold axis of symmetry. The possibility of cubic symmetry was eliminated by the metallography since the microconstituent changed color during rotation when the incident light was plane polarized.

Evidence for allotropy in the crystal structure of $TiAu_2$ was not found. The microconstituent of this phase always appeared to be the same when viewed with polarized light. Furthermore, it should be noted that Widmänstatten markings were not observed. X-ray powder diffraction data obtained from $TiAu_2$ specimens which had been heat-treated at 900, 760, 600 and 400°C, and subsequently quenched into liquid argon all yield the same diffraction maxima. These data were utilized to determine the crystal structure of this intermediate phase.

Debye-Scherrer X-ray powder diffraction data were indexed in the tetragonal system, see Table V . Lattice parameters were computed by Cohen's method with the Datatron which is manufactured by the Electrodata Corporation. The input data included 35 measured maxima which had been obtained with both copper and cobalt radiation.

$$a = b = 3.4192 \pm 0.0003\text{Å}, \quad c = 8.5137 \pm 0.0003\text{Å}$$

$$c/a = 2.490$$

An examination of the indexing of the data in Table V indicates the presence of a body centered tetragonal lattice:

$(hk\ell)$ observed only if $h + k + \ell = 2n$

Space groups in the tetragonal system which are compatible with the systematic absences are D_{4h}^{17}, D_{2d}^{11}, D_{2d}^{9}, C_{4v}^{9}, D_{4}^{9}, C_{4h}^{5}, C_{4}^{5}, and S_{4}^{2}. The atomic content of a unit cell was established as 2 titanium atoms and 4 gold atoms from the lattice parameters and measured density of 15.6 gm cm^{-3} which yield n = 2.13 molecules. It was not possible to explain the observed data by placing all the atoms in special positions. However, the observation that the strongest diffraction maxima occur for $(hk\ell)$ in which ℓ = 0, 1, 2, 3 does suggest a motif in which those atoms which have a large cross-section for the scattering of X-rays are in equivalent positions possessing a variable parameter which is approximately 1/3. A trial structure was obtained from atomic packing considerations. The disposition of atoms is common to space groups D_{4h}^{17}, D_{2d}^{11}, D_{2d}^{9}, D_{4}^{9}, C_{4h}^{5}, and S_{4}^{2}; therefore the atomic positions which have been specified are for the space group of highest symmetry, D_{4h}^{17}-I4/mmm:

2 Ti in (a): 0,0,0; 1/2,1/2,1/2.

4 Au in (e): 0,0,z; 0,0,$\bar{z}$; 1/2,1/2,1/2+z; 1/2,1/2,1/2+$\bar{z}$
with z 1/3

Structure factor calculations disclosed that $\Delta F/\Delta z$ was extremely small for those $(hk\ell)$ in which $\ell = 3, 6, 9$. For the (hk0) diffraction maxima, $\partial F(hk0)/\partial z$ is obviously zero for this particular motif of atoms; and one may use these spectra to compute the coefficient of the temperature factor. This was done in the usual manner by plotting $\ln (I_{calc.}/I_{obs.})$ as a function of $\sin^2\theta/\lambda^2$. The calculated intensity included contributions from the Lorentz and polarization factors LP, the square of the structure factor $F^2(hk\ell)$, an absorption correction $A(\mu r,\theta)$ for a powder rod of characteristic $\mu r = 8$, and a multiplicity factor p. Data from the (110), (200), (220), and (310) spectra were employed for this purpose and the slope of the resulting straight line yield a temperature factor coefficient $B = 1.83\ \mathring{A}^2$.

The ability of the trial structure to explain the observed intensities was encouraging and an attempt was made to determine the positional parameter more accurately since the crystal structure is relatively simple. We have already mentioned one of the important features of this atomic arrangement: namely that $\Delta F(hk\ell)/\Delta z$ is very small for the very intense spectra, over the positional parameter interval which is sanctioned by packing considerations. Thus an investigation of the medium and weak spectra might suffice to establish our objective. Structure factors were computed for 0.001 increments in the positional parameter from z = 0.328 to

$z = 0.343$. Relative intensities were calculated with the expression:

$$I_{Rel.Calc.} = \text{constant } PLF^2(hk\ell)A(\mu r,\theta)p\exp(-B\sin^2\theta/\lambda^2)$$

The best agreement for those maxima which were sensitive to changes in z indicated this parameter to be 0.337, the agreement between observed and calculated relative intensities at this value of z is shown in figure 14. Reasonably good agreement occurs over the interval 0.336 to 0.339. Interatomic distances of atoms in $TiAu_2$ are given in Table VI, the positional parameter being taken as 0.337.

The Crystal Structure of the Intermediate Phase $TiAu_4$

In this section we shall describe the crystal structure of $TiAu_4$ and its relationship to the terminal alpha phase. We shall make use of matrix algebra and describe our basis vectors in the nomenclature recommended by the International Union of Crystallography (10). Let us recall that the space lattice of the alpha phase is defined by the orthogonal base vectors $\vec{a}_1$, $\vec{b}_1$, $\vec{c}_1$ which are equal in magnitude. The motif of any particular unit cell consists of four statistical atoms located at the corners and face-centers.

The X-ray powder diffraction photographs of $TiAu_4$ disclosed a pattern consisting of a few strong and many relatively weak maxima. When one considers the chemical composition of

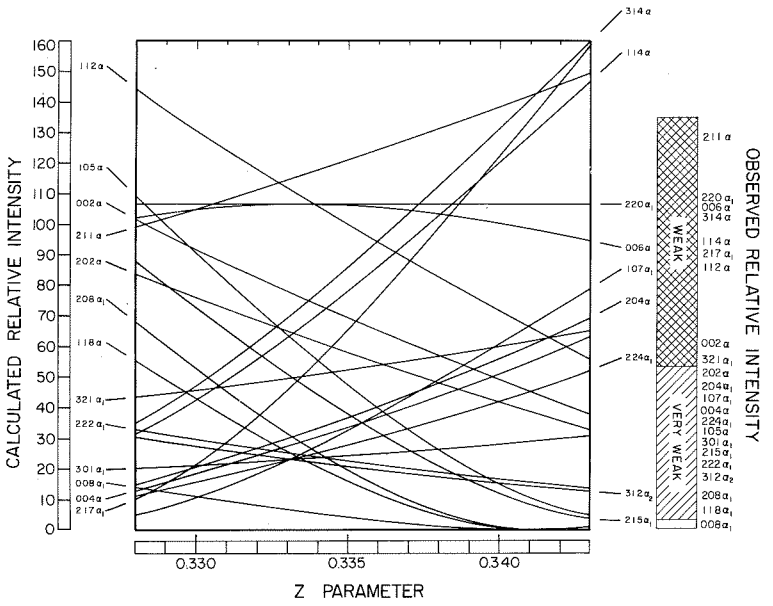

FIG. 14. CALCULATED RELATIVE INTENSITIES FOR THE CRYSTAL STRUCTURE OF $TiAu_2$. POSITIONAL PARAMETER VARIATION FROM 0.328 TO 0.343. COPPER Kα RADIATION.

the phase it is clear that the gold atoms contribute most to the scattering of X-rays. Thus we conclude that a crystal structure based on consideration of only the strong maxima may lead to a trial or approximate structure which could indeed be close to the actual distribution of electron density which must explain all spectra, strong and weak. We shall approach the problem in this manner, first formulating a pseudo cell, so that the nature of the difficulty that is encountered may be seen clearly. Here our motivation for determining the phase relationships between $TiAu_4$ and alpha becomes clear in the light of previously reported X-ray results (5). Finally we shall write the transformations which are necessary to describe the lattice of $TiAu_4$ in terms of this virtual lattice. If justification for such a procedure is necessary let it be found in the knowledge that this was in fact the method used to determine the crystal structure of this intermediate phase.

The positions and relative intensities of the strongest maxima in the $TiAu_4$ diffraction pattern suggest a face-centered tetragonal lattice. We relate the space lattice of the cubic alpha phase in object space to the space lattice of the pseudo or virtual unit cell by the linear transformation,

$$\begin{vmatrix} a_p \\ b_p \\ c_p \end{vmatrix} = \begin{vmatrix} \eta_{11} & 0 & 0 \\ 0 & \eta_{22} & 0 \\ 0 & 0 & \eta_{33} \end{vmatrix} \begin{vmatrix} a_1 \\ b_1 \\ c_1 \end{vmatrix}$$

From symmetry requirements we may write:

$$\eta_{11} = \eta_{22} \neq \eta_{33} .$$

Measurement of the positions of strong maxima indicate

$$\eta_{11} > 1 \quad \text{and} \quad \eta_{33} < 1 .$$

The lattice of the pseudo cell is tetragonal and the matrix coefficients η_{11} and η_{33} are such that:

$$a_p = b_p = 4.08\text{Å} \quad \text{and} \quad c_p = 3.98\text{Å},$$

$$c_p/a_p = 0.975 .$$

The unit cell of $TiAu_6$ described in the literature by Raub, Walter, and Engel is equivalent to our description of the pseudo cell for $TiAu_4$.

The primary crystals of $TiAu_4$ did not exhibit well defined faces in the microstructures, figure 4. There is, however, a spike-like appearance to the crystal form which could result from the incomplete development of double pyramids of the first, second, or third kind in the tetragonal system (11). If we consider the crystal morphology as an expression of the reciprocal lattice it is then clear that the crystal form in object space must represent a solid geometrical figure of axial ratio less than one. This observation was used to index the entire

powder diffraction pattern of $TiAu_4$ with a Hull Davey chart. All interplanar spacings were marked off on a paper strip and the (002) spacing of the pseudo cell was made to coincide with the (002) curve on the Hull Davey chart as the observed data were moved to smaller values of c/a. A matching of the observed data to the chart was obtained and the matrix which relates the unit vectors of $TiAu_4$ to the unit vectors of the pseudo cell can be written:

$$\begin{vmatrix} a_2 \\ b_2 \\ c_2 \end{vmatrix} = \begin{vmatrix} \gamma_{11} & \gamma_{12} & 0 \\ \gamma_{21} & \gamma_{22} & 0 \\ 0 & 0 & \gamma_{33} \end{vmatrix} \begin{vmatrix} a_p \\ b_p \\ c_p \end{vmatrix}$$

The manner in which the indexing was performed indicates that $\eta_{33} = \gamma_{33}$. A schematic representation of this transformation is to be found in figure 15; here the unique axis of the tetragonal systems is normal to the plane of the paper. The remaining four matrix coefficients are easily determined

$$\gamma_{11} = 3/2, \quad \gamma_{22} = 3/2 \ , \ \gamma_{21} = 1/2, \text{ and}$$

$$\gamma_{12} = - 1/2.$$

Evaluation of the matrix yields the unit cell content, $V_2 = 5/2\ V_p = 10$ atoms. Although the atomic motif has not yet been determined it can be seen that the crystallographic transformation of axes does confirm the stoichometric composition as established by optical metallography. Since

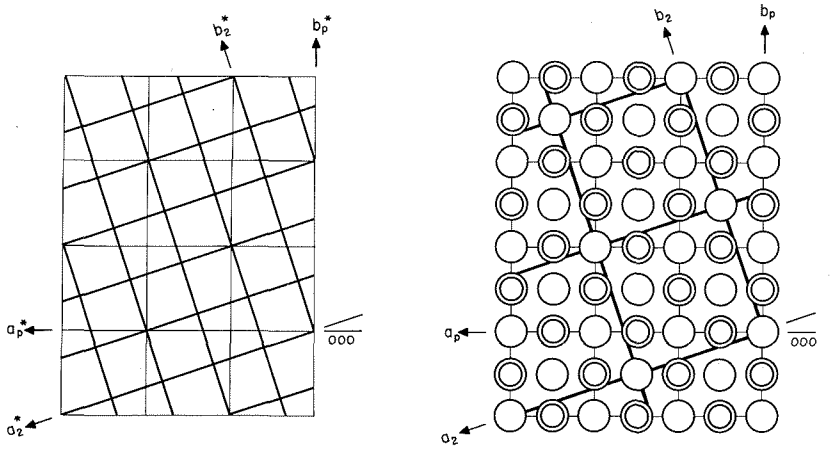

(a) (b)

FIG. 15. ORIENTATION RELATIONSHIPS OF THE INTERMEDIATE PHASE $TiAu_4$ AND A PSEUDO TETRAGONAL LATTICE IN (a) RECIPROCAL SPACE AND (b) IN OBJECT SPACE.

$\gamma_{33} = \gamma_{33}$ we observe that transformation of axes in two dimensions is a conformal transformation and we may write the reduced gamma matrix as the product of a dilitation and rotation:

$$\begin{vmatrix} \gamma_{11} & \gamma_{12} \\ \gamma_{21} & \gamma_{22} \end{vmatrix} = \begin{vmatrix} r_o & 0 \\ 0 & r_o \end{vmatrix} \begin{vmatrix} \cos\Omega & -\sin\Omega \\ \sin\Omega & \cos\Omega \end{vmatrix}$$

where $\Omega = 18°30'$ and $r_o = a_2/a_p$. Indexing of the observed diffraction maxima for $TiAu_4$ is given in Table VII. The observed reflections indicate only one systematic extinction, i.e.: $(hk\ell)$ present only if $h + k + \ell = 2n$, a body-centered tetragonal space lattice.

To obtain a trial structure we write the relationships between axes in reciprocal space, see figure 15.

$$\begin{pmatrix} a_2^* \\ b_2^* \\ c_2^* \end{pmatrix} = \begin{pmatrix} \beta_{11} & \beta_{12} & 0 \\ \beta_{21} & \beta_{22} & 0 \\ 0 & 0 & \beta_{33} \end{pmatrix} \begin{pmatrix} a_p^* \\ b_p^* \\ c_p^* \end{pmatrix}$$

Where we have the following values for the coefficients:

$$\beta_{11} = \beta_{22} = 3/5,\ \beta_{21} = -\beta_{12} = 1/5, \text{ and } \beta_{33} = 1$$

The transformation of axes in reciprocal space yields atomic sites for the trial crystal structure; these ideal positions

are then to be observed in the object space of figure 15. We shall summarize the results of this transformation with the notation of the International Tables for X-Ray Crystallography (10).

0,0,0; 1/2,1/2,1/2

+ 2 Ti :(a) 000

+ 8 Au :(h) x,y,0; $\bar{x},\bar{y},0$; $\bar{y},x,0$; $y,\bar{x},0$.

with x = 0.200

y = 0.400

This ideal disposition of atoms is in space group C_{4h}^5-I4/m. Other possible space groups for this crystal structure, which do not require large changes in atomic positions, necessitate the introduction of one and two z parameters; these are S_4^2-I$\bar{4}$ and C_4^5-I4.

It is clear that a trial crystal structure derived in such a manner will of necessity yield the correct values of intensities for strong maxima. The correctness of the proposed motif of atoms then rests on how well the relatively weak intensities are explained. The space group of highest symmetry was used as a starting point for the structure determination. One may see a reason for this procedure in the diffraction indexing of Table VII. Small variations in the x and y parameters will result in large phase changes since

the h,k indices are numerically larger than those associated with the unique axis in the tetragonal system. Attenuation of X-rays in the powder rod, which was used for diffraction experiments, was considerable since $\mu r = 15$ for the cobalt radiation. An absorption correction $A(\mu r, \theta)$ was included in the calculations for relative intensities as were the usual Lorentz, polarization, and multiplicity factors. The ideal positions of atoms did not explain all weak spectra correctly and for this reason the variation of the structure factor with changes in x and y were investigated for all $(hk\ell)$ within the sphere of reflection. Two dimensional plots indicating the change in structure factor with positional parameters covered the region $0.180 \leq x \leq 0.220$ and $0.380 \leq y \leq 0.420$. Consideration of these calculations led to the following parameters:

$$x = 0.200 \pm 0.001 \text{ and } y = 0.3970 \pm 0.0008.$$

It was not possible to improve the agreement between observed and calculated relative intensities by introducing a z parameter. Interatomic distances for atoms in the crystal structure of $TiAu_4$ are presented in Table VIII.

An interesting feature of this crystal structure determination is that on the basis of the powder diffraction data indexing alone one should consider space groups in the Laue-symmetry groups 4/m and 4/mmm. Yet the transformation of axes, which we know will yield a trial structure which is

close to the correct crystal structure, directs us to the space groups of Laue-symmetry group 4/m. It is clear that the Laue X-ray experiment, performed on a single crystal of $TiAu_4$, would be a critical test of our intuitive approach to this problem. The grain size of homogenized specimens of $TiAu_4$ is very small, figure 9; the possibility of obtaining a single crystal, useful for diffraction studies, from such an aggregate is not encouraging. However, it was possible to obtain single crystals of the order of 0.1mm by the following procedure. An alloy containing 84 atomic percent gold was heat-treated at 1150°C for ten days. From the constitution diagram we observe that the alloy will be in a region of $TiAu_4$ plus liquid. The length of annealing time was selected so as to promote grain growth of the solid phase. Having made such an alloy we draw upon our understanding of the metallography of these alloys and recall that the liquid phase will crystallize as a continuous series of solid solutions of titanium in gold. Our problem is to remove the large grains of $TiAu_4$ from the network of ductile alpha at the grain boundaries. This was accomplished by making the gold-rich phase form an amalgam with mercury, after which the large polyhedral grains of $TiAu_4$ could be selected with ease.

Laue photographs of one such single crystal are shown in figures 16a and 17. In this manner the crystal structure of $TiAu_4$ is shown to belong to the symmetry group 4/m. There is a very pleasing relationship between $TiAu_4$ and a simple face-

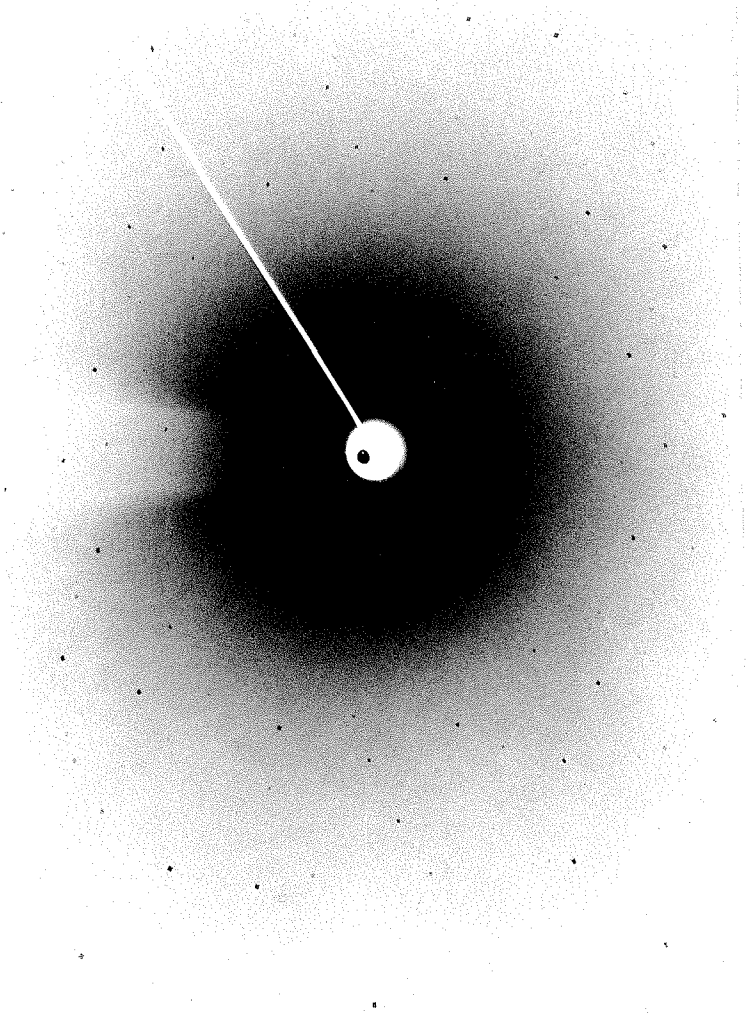

Fig. 16a.--Laue photograph of a single crystal of $TiAu_4$. Transmission.

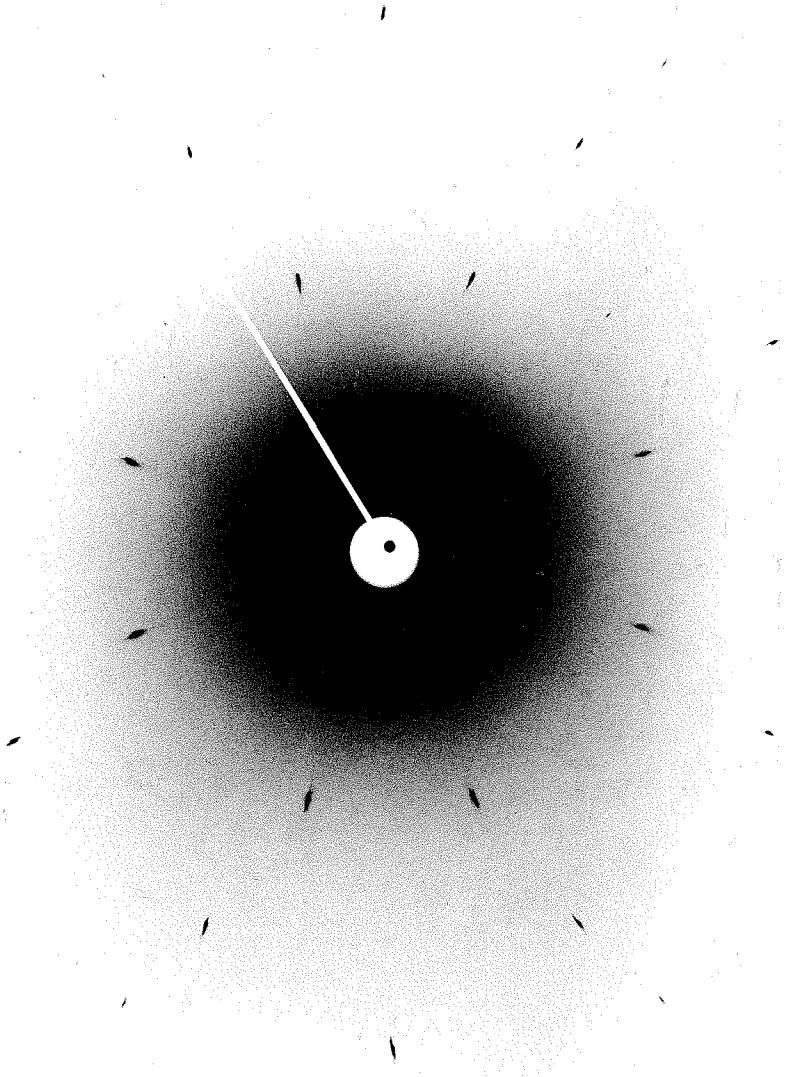

Fig. 16b.--Laue photograph of a single crystal of copper. Transmission.

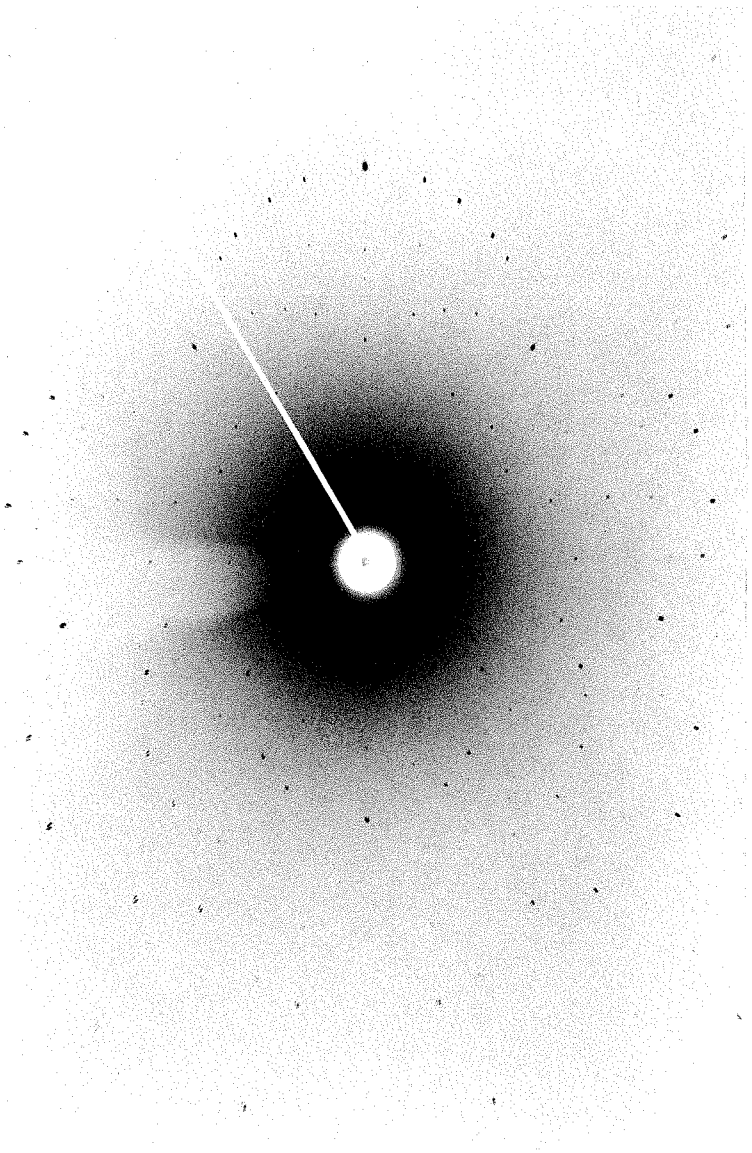

Fig. 17.--Laue photograph of a single crystal of $TiAu_4$. Transmission.

centered cubic metal. This can be seen clearly by performing the Laue experiment, for each crystal, with the incident beam directed along the four-fold axis. A vapor deposited regular octahedra of copper was selected for the face-centered cubic metal. The Laue symmetry is displayed in figure 16b. A study of these four-fold Laue photographs yields the understanding of the linear transformations which we have performed. Figure 18 shows the gnomonic projections of figures 16a,b. The indexing is in agreement with our previous statements and we observe that we are able to deduce Ω for the conformal transformation. The projection distance for the copper crystals' Laue photograph would have to be suitably normalized before r_o could be established.

We have already mentioned the fact that from powder diffraction data alone it was necessary to introduce only two parameters of position for the gold atoms. A further confirmation of this observation was obtained from the single crystal of $TiAu_4$. A rotation photograph about [001] was made with MoKα and it was noted that all odd layer lines were identical, as was the case for all even layer lines.

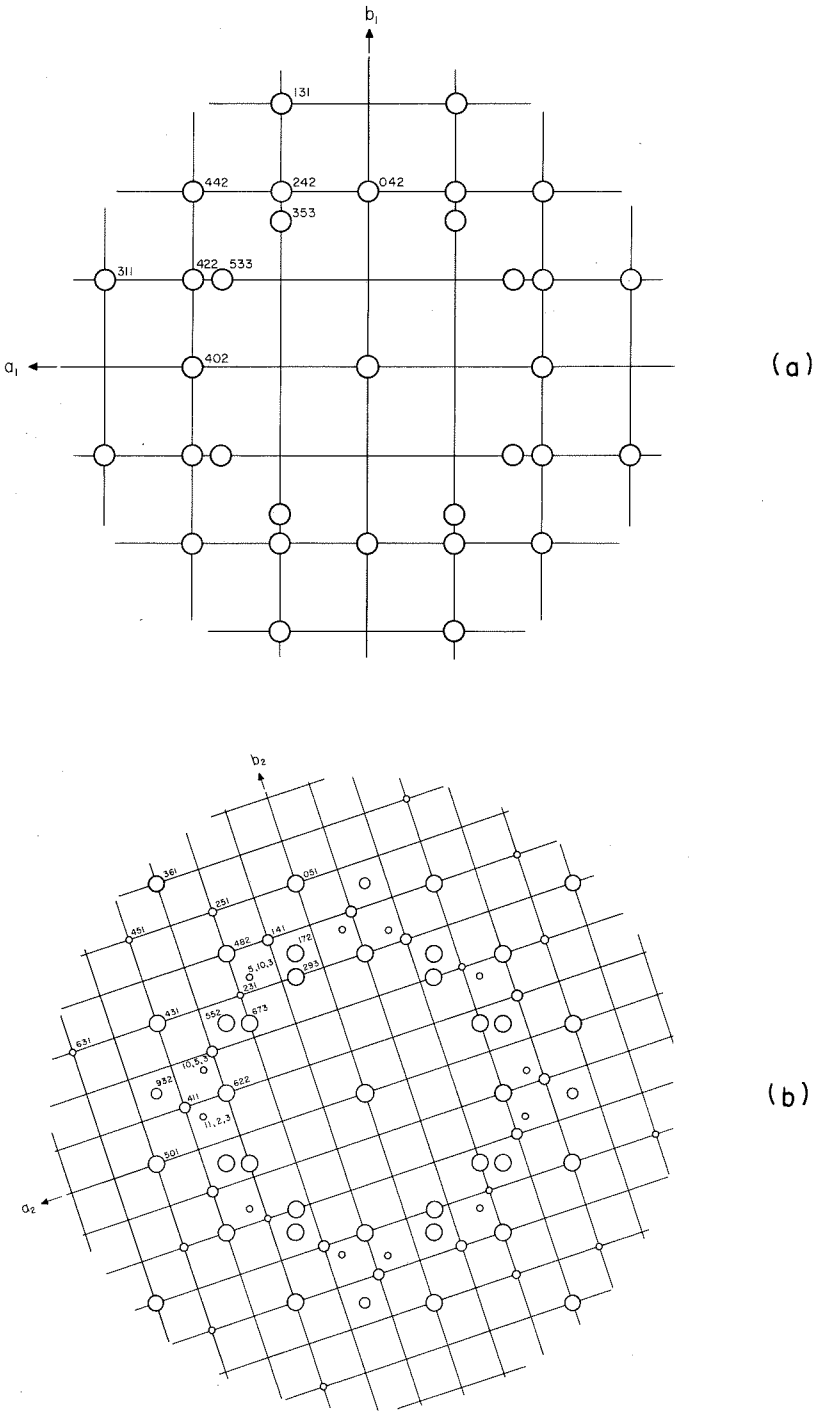

FIG. 18. GNOMONIC PROJECTIONS OF (a) COPPER AND (b) $TiAu_4$ WITH THE 4-FOLD SYMMETRY AXES NORMAL TO THE PLANE OF PROJECTION.

DISCUSSION

The partial constitution diagram as determined by this investigation is similar in form to that proposed by Raub et al. (5). Both experimental studies failed to yield evidence for the intermediate phase $TiAu_3$ which was reported by Wallbaum (4). There is reasonable agreement on the reported values of the peritectic temperatures: 1115°C and 1190°C were the values reported by the previous investigation, 1123 $\pm$ 3°C and 1172 $\pm$ 5°C are the present results.

There are several major differences in the phase relationships which have proposed by the two investigations. These are the limit of solubility of titanium in the alpha solid solutions and secondly, the composition and region of homogeneity over which the gold-rich intermediate phase does exist. With respect to the former it is interesting that the X-ray diffraction results of both investigations show the same negative linear deviation from Vegard's law; Raub et al. have located the temperature dependent alpha phase boundary from metallographic evidence. The maximum solubility measured was 8.5 atomic percent titanium at 1000°C. Although some difficulties were encountered in the X-ray diffraction experiments, by the same authors, the extrapolated value of the maximum solubility of titanium was determined to be 10.3 atomic percent at the peritectic temperature, 1115°C. Results

of the present study indicate that 12 atomic percent titanium is soluble in face-centered cubic alpha at 1100°C, a fact which is confirmed by the X-ray powder diffraction photograph of filings quenched from this temperature into liquid argon. Extrapolation of the metallography data places the maximum solubility at approximately 13 atomic percent titanium at the peritectic temperature, 1123°C. The intermediate phase which we have designated $TiAu_4$, and which does exist over the composition interval 79 to 82 atomic percent titanium, has the same characteristic microstructure as the $TiAu_6$ phase of Raub et al. To illustrate this point let the reader compare figure 9 of this text with figure 12 in reference 5. The crystal structure determination also confirms $TiAu_4$ as a correct description of the composition of the gold-rich intermediate phase. It may be of value to reiterate a point which has already been touched upon: the X-ray diffraction results reported in the literature for $TiAu_6$ represent a pseudo lattice which is related to the space lattice of $TiAu_4$. It must be conceded however that the reported tetragonal space lattice for $TiAu_6$ could be that of a metastable phase and thus represent non-equilibrium conditions. The thermal analysis data of the previous investigation (5) does indeed include evidence to support our contention that $TiAu_4$ is the stoichiometric composition of the first intermediate phase. Thus in figure 1 thermal arrests at approximately 1115°C were observed in alloys containing 16.8, 18.4, and 21.3 atomic percent titanium.

The previously reported hexagonal close-packed lattice of $TiAu_2$ (5) has not been confirmed. We have found the lattice to be body-centered tetragonal and the crystal structure to be of the $MoSi_2$ type (12). Other isomorphous compounds of this atomic motif are WSi_2 (12), Cr_2Al (13), Hg_2Mg (14), and $ReSi_2$ (15). It is interesting that the reported values of the positional parameter vary from 0.319 in the case of Cr_2Al to 0.333 for Hg_2Mg and the silicides.

The crystal structure of $TiAu_4$ is isomorphous with $MoNi_4$ (16) and WNi_4 (17). In the latter crystal structure determinations the positional parameters were determined to be x = 0.200 and y = 0.400. These are the ideal positions of atoms as determined by the linear transformation of axes in reciprocal space. It is indeed interesting that in the case of $TiAu_4$ it was necessary to move the atoms in the eight-fold positions away from the ideal sites in order to make the calculated intensities agree with the observed intensities. Here too, the atoms with relatively weak scattering power are in special positions, a situation which increases our ability to locate the gold atoms which are associated with the variable parameters of position. The axial ratios, c_2/a_2, for $MoNi_4$, WNi_4, and $TiAu_4$ are close in value: 0.623, 0.620, and 0.616. Furthermore we observe that the axial ratios for the pseudo cells are in agreement $c_p/a_p = 0.98$.

Let us now consider a very important aspect of the physical metallurgy of $TiAu_4$ and its relationship to the titanium-gold

phase diagram. When it was discovered that $TiAu_6$ did not exist and that $TiAu_4$ possessed a crystal structure which was closely related to the face-centered cubic solid solution a new problem did arise. The systems nickel-tungsten (18) and nickel-molybdenum (19) both display this ordered phase, but in these constitution diagrams it is clear that the intermediate phase of the A_4B type does arise from a peritectoid reaction. In our symbolic notation A is a face-centered cubic metal. Much of the effort expended in the present investigation was for the sole purpose of finding the phase relationships of $TiAu_4$ in the region of the peritectic temperatures so as to make certain the postulated phase equilibria were correct. No evidence was found which might lead one to suspect that $TiAu_4$ formed from a solid state reaction. One may inquire into the origin of the markings which are observed in this phase; these have also been observed in WNi_4 (see figure 8d of reference 17). It is certainly pertinent to the present discussion to question these striations as evidence of a solid state reaction. We shall not take this matter any further at the present time, since it represents a complete investigation in itself, but comment that our experiments do suggest that these lines are the result of preferential etching along specific crystallographic directions.

Table I. Chemical Analysis of Several Titanium-Gold Alloys

Nominal Composition (Atomic %)	Chemical Analysis (Atomic %)	(Weight %)
98	97.8	99.5
96	96.2	99.1
94	93.9	98.5
92	91.9	97.9
90	90.3	97.4

Chemical analysis performed by Smith-Emery Co. of Los Angeles. Analysis numbers 406005-9 and 406533.

Table II. Thermal History of the Titanium-Gold Alloys

Temperature °C	Time of Heat Treatment
Above 1100	5-30 minutes
1100	30 minutes
1050	30 minutes
1000	30 minutes to 48 hours
900	48 hours
850	5 days
800	10 days
700	12 days
600	14 days
400	30 days
370	30 days

Table III. Lattice Parameters of Gold and the Face-Centered Cubic Alpha Solid Solutions of Titanium-Gold Alloys

Gold Content Atomic %	Annealing Temperature °C	X-Radiation	Method of Analysis *	Lattice Parameter Å	Atomic Volume $(Å)^3$
100.0		Cu Kα	C	4.078(3)	16.96
100.0		Co KαKβ	C	4.078(1)	16.96
97.8	800	Co Kα	C	4.076(3)	16.93
97.8	1000	Co KαKβ	N-R	4.076(9)	16.94
97.8	1000	Cu Kα	N-R	4.076(8)	16.94
96.2	800	Co Kα	C	4.074(6)	16.91
96.2	1000	Cu Kα	N-R	4.075(0)	16.92
93.9	800	Co Kα	C	4.071(8)	16.88
93.9	1000	Co KαKβ	N-R	4.072(1)	16.88
93.9	1000	Cu Kα	N-R	4.072(1)	16.88
91.9	1000	Co KαKβ	N-R	4.070(5)	16.86
91.9	1000	Cu Kα	N-R	4.070(6)	16.86
90.3	1000	Co KαKβ	N-R	4.068(2)	16.83
90.3	1000	Cu Kα	N-R	4.068(3)	16.83
88	1100	Co KαKβ	N-R	4.065(3)	16.80

*The method used to derive the extrapolated lattice parameter was either that due to M. Cohen (7) or Nelson and Riley (9) as the abbreviation in this column of the table indicates.

Table IV. Lattice Parameters of the Intermediate Phase $TiAu_4$. Debye-Scherrer Photographs made with Cobalt Kα Radiation.

Gold Content Atomic %	Annealing Temperature °C	Lattice Parameters in Å $a_2 = b_2$	c_2	Axial Ratio c_2/a_2	Atomic Volume $(Å)^3$/atom
84	600	6.458(8)	3.983(8)	.6168	16.62
84	800	6.458(1)	3.988(0)	.6175	16.63
84	1100	6.457(7)	3.986(8)	.6174	16.63
82	600	6.459(8)	3.980(6)	.6162	16.61
82	800	6.458(2)	3.983(0)	.6167	16.61
82	1100	6.457(0)	3.986(3)	.6174	16.62
80	600	6.460(7)	3.975(8)	.6154	16.60
80	800	6.457(8)	3.976(0)	.6157	16.58
80	1100	6.461(0)	3.977(1)	.6155	16.60
78	600	6.459(9)	3.972(4)	.6149	16.58
78	800	6.461(5)	3.968(9)	.6142	16.57
75	370	6.460(7)	3.971	.6146	16.58
75	950	6.461(8)	3.973	.6148	16.59
70	370	6.461(8)	3.973	.6148	16.57

Table V. Debye-Scherrer Powder Diffraction Data for the Intermediate Phase $TiAu_2$. Copper Kα Radiation. Calculated Relative Intensities of the Crystal Structure of $TiAu_2$ with the Positional Parameter z equal to 0.337.

hkℓ		$Sin^2\theta$ Observed	$Sin^2\theta$ Calculated	Relative Intensity Observed*	Relative Intensity Calculated (z = 0.337)
002	α	0.03371	0.03477	W	61
101	α	0.05943	0.06047	M	220
110	α	0.10237	0.10270	S	585
103	α	0.12529	0.12557	VS	1000
004	α	0.13172	0.13206	VW	40
112	α	0.13504	0.13533	W	88
200	α	0.20413	0.20398	M	309
114	α	0.23356	0.23343	W	94
202	α	0.23771	0.23670	VW	51
105	α	0.25729	0.25634	VW	32
211	α	0.26357	0.26289	W	129
006	α	0.29599	0.29563	W	105
213	α	0.32965	0.32838	VS	754
204	α_1	0.33540	0.33493	VW	44
116	α_1	0.39776	0.39650	M	212
220	α_1	0.40734	0.40632	W	107
222	α_1	0.44098	0.43903	VW	20
107	α_1	0.45347	0.45210	VW	43

Table V (continued)

hkℓ		$Sin^2\theta$ Observed	$Sin^2\theta$ Calculated	Relative Intensity Observed*	Relative Intensity Calculated (z = 0.337)
215	α_1	0.45903	0.45865	VW	26
301	α_1	0.46669	0.46520	VW	26
206	α	0.49930	0.49791	M_B	280
310	α	0.50977	0.50859	M_B	280
008	α		0.52557	A	2
303	α	0.53192	0.53153	M_B	278
224	α_1	0.53818	0.53717	VW	33
312	α_2	0.54167	0.54314	VW	19
118	α_1	0.62790	0.62550	VW	8
314	α	0.64000	0.63968	W_B	103
217	α_1	0.65667	0.65496	W	88
321	α_1	0.66839	0.66806	W	56
226	α_1	0.70146	0.70077	M	210
109	α_1	0.71463	0.71385	M	209
208	α_1	0.72900	0.72955	VW	10

*Observed intensities are designated as follows: VVS, very very strong; VS, very strong; S, strong; M, medium; W, weak; and VW, very weak. The letter A indicates that a reflection was not observed for the corresponding (hk). The subscript B which is introduced in the observed relative intensity column is used to show that the diffraction maxima was relatively diffuse.

Table VI. Interatomic Distances for the Intermediate Phase $TiAu_2$.

Atom	Neighbors	Distance Å
Ti(a)	8 Au(e)	2.79
	2 Au(e)	2.86
	4 Ti(a)	3.419
Au(e)	4 Ti(a)	2.79
	1 Au(e)	2.79
	4 Au(e)	2.83
	1 Ti(a)	2.86

Table VII. Debye-Scherrer Powder Diffraction Data for the Intermediate Phase $TiAu_4$. Cobalt Kα radiation. Calculated Relative Intensities of the Crystal Structure of $TiAu_4$ with x = 0.200 and y = 0.397.

hkℓ		$\sin^2\theta$ Observed	$\sin^2\theta$ Calculated	Relative Intensities Observed*	Relative Intensities Calculated
110	α	.0380	.0384	W	1875
101	α	.0693	.0695	W	2296
200	α	.0768	.0767	W	1364
121	α	.1467	.1462	VS	87953
220	α		.1535	A	499
310	α	.1914	.1919	S	36423
002	α	.2012	.2012	M	6154
301	α	.2254	.2230	A	771
112	α	.2405	.2396	VW	910
202	α	.2790	.2779	VW	1172
321	α	.2998	.2997	W	2163
400	α		.3070	A	569
330	α	.3448	.3453	VW	621
222	α	.3560	.3547	VW	602
411	α	.3763	.3765	W	1131
420	α	.3831	.3837	M	23457
312	α	.3924	.3931	S	46477
103	α	.4736	.4719	VW	668
510	α	.4986	.4989	VW	1020
402	α	.5082	.5082	VW	838
501	α_1	.5293	.5300	VS	13035
431	α_1	.5293	.5300		26071
332	α_1		.5465	A	681
213	α_1	.5486	.5486	S	26274
422	α_1	.5849	.5849	S	23681
521	α_1	.6067	.6067	W	1300
440	α_1		.6140	A	247
303	α_1		.6253	A	323
530	α_1		.6524	A	227
600	α_1		.6908	A	146

Table VII (continued)

hkℓ		$\sin^2\theta$ Observed	$\sin^2\theta$ Calculated	Relative Intensities Observed*	Relative Intensities Calculated
512	α_1	.7010	.7001	W	1286
323	α_1	.7024	.7021	W	1023
611	α_1		.7602	A	537
620	α_1	.7673	.7675	M	13170
413	α_1	.7795	.7789	W	653
004	α_1	.8061	.8061	WM	5083
004	α_2	.8149	.8096	W	2042
442	α_1	.8149	.8152		569
531	α_1	.8360	.8370	VW	790
114	α_1	.8442	.8445	A	508
532	α_1	.8532	.8536	VW	863
204	α_1	.8825	.8828	W	1234
204	α_2	.8912	.8873	W	617
602	α_1	.8912	.8920		752
361	α_1	.9130	.9137	VS	74326
503	α_1	.9297	.9324	VVS	44227
433	α_1	.9297	.9324		88313
710	α_1	.9584	.9594		3273
550	α_1	.9584	.9594	S	30630
224	α_1	.9584	.9595		1587
622	α_1	.9684	.9687	VVS	137222
701	α_1	.9901	.9904	M	8063

*Observed intensities are designated as follows: VVS, very very strong; VS, very strong; S, strong; M, medium; W, weak; and VW, very weak. The letter A indicates that a reflection was not observed for the corresponding (hk). The subscript B which is introduced in the observed relative intensity column is used to show that the diffraction maxima was relatively diffuse.

Table VIII. Interatomic Distances for the Intermediate Phase $TiAu_4$. Calculated for a Composition of 80 Atomic Percent Gold.

Atom	Neighbors	Distance Å
Ti in (a)	8 Au	2.854 ± 0.006
	4 Au	2.871 ± 0.007
Au in (h)	2 Au	2.823 ± 0.010
	2 Ti	2.854 ± 0.006
	4 Au	2.859 ± 0.011
	1 Ti	2.870 ± 0.008
	2 Au	2.897 ± 0.016
	1 Au	2.905 ± 0.017

PART II

LONG-RANGE ORDER IN TiFe, TiCo, and TiNi

INTRODUCTION

Let us consider the intermediate phases of equi-atomic proportions which result from alloying titanium with neighboring elements belonging to the scandium transition metals. A sigma phase of composition TiMn has been reported in the titanium-manganese system (20). The phases TiFe, TiCo, and TiNi were found in an early investigation (21) and described as CsCl type crystal structures; but neither lattice parameters nor intensity data were presented to support this statement. A later experimental investigation yielded lattice parameter measurements for TiFe, TiCo, and TiNi but did not establish these phases as the CsCl type (22); cobalt Kα radiation was used for the Debye-Scherrer powder diffraction studies. Finally we shall mention a recent paper in which the authors sought to resolve the question of ordering with the use of chromium Kα radiation (23). This attempt was not successful.

The present investigation is concerned with ascertaining if long-range order does exist in TiFe, TiCo, and TiNi. In essence this is the problem of determining whether the atomic motif is to be described by a random distribution of all atoms at corners and centers of the cubic space lattice or if the individual atomic species display a preference for specific sites.

DISCUSSION

The equi-atomic phases TiFe, TiCo, and TiNi contain two atoms per unit cell which are in the special positions: (a) 0,0,0 and (b) 1/2,1/2,1/2. The crystal structure is of the wolfram type, A2, if complete disorder of atoms does exist amongst both crystallographic sites. Long-range order, which implies that each particular species of atoms occupies equivalent sites in the space lattice, results in the cesium chloride type crystal structure, B2. If we designate these three intermediate phases by the generalized formula TiM then the former spatial configuration of atoms yields a non-vanishing structure factor when the sum of the Miller indices is even; its magnitude is equal to the sum of the atomic scattering factors: $F_{(e)}(hk\ell) = f_M + f_{Ti}$. The latter distribution of atoms will result in a similar structure factor when $h + k + \ell = 2n$, where $n = 0, 1, 2, \ldots .$; however, if $h + k + \ell = 2n + 1$ we then observe that $F_{(o)}(hk\ell) = f_M - f_{Ti}$. Thus the existence of complete order may be substantiated by observing relatively weak diffraction maxima whose intensities are proportional to $F_{(o)}(hk\ell)F_{(o)}(hk\ell)^*$.

Having seen the importance of increasing the difference in atomic scattering factors, let us now consider how anomalous dispersion may be used in this respect. This phenomenon is most pronounced when the frequency of the incident radiation is in the neighborhood of the characteristic frequency of

oscillators in the matter. We shall designate by f_0 the atomic scattering factor which is obtained from a model such as the Thomas-Fermi, Hartree, or Pauling-Sherman charge distributions and remark parenthetically that its magnitude is known precisely only in the direction of the incident beam. Here it has a value which is equal to the atomic number of the scatterer. For the general case of scattering by a many-electron atom we can write

$$f = f_0 + \Delta f_k' + i\, \Delta f_k''$$

where $\Delta f_k'$ and $\Delta f_k''$ are the real and imaginary corrections which may be obtained from the quantum-mechanical dispersion theory for K electrons which is due to Hönl (24). The qualitative features of the anomalous dispersion of X-rays may be seen in figure 19 which is taken from R. W. James (25). On the low energy side of $\lambda = \lambda_k$ the scattering factor is real, whereas when the wavelength of the incident radiation is less than λ_k the scattering factor is a complex quantity. It is important to note that $\Delta f_k''$ changes with the parameter $\sin\theta/\lambda$, this is not the case for $\Delta f_k'$. These observations have resulted from experiment and may be deduced from the theory.

To obtain an order of magnitude for the variation in atomic scattering factor with wavelength of incident wavelength let us determine these quantities for $\sin\theta/\lambda = 0.17\text{Å}^{-1}$ using

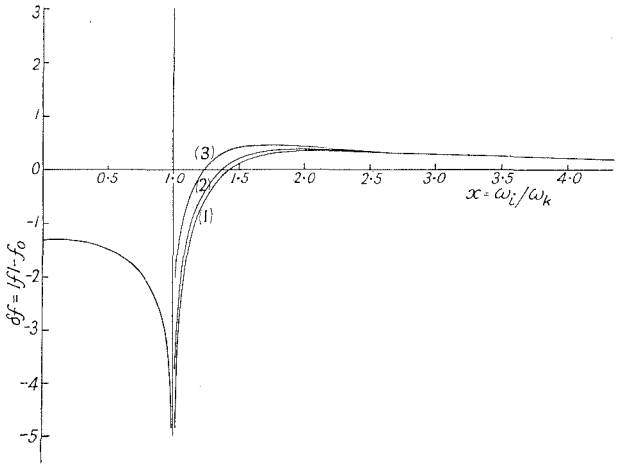

FIG. 19. ILLUSTRATING THE EFFECT OF AN IMAGINARY COMPONENT $\Delta f''$ OF THE SCATTERING FACTOR. δf IS PLOTTED AS A FUNCTION OF ω_i/ω_k FOR THE K ELECTRONS OF THE IRON ATOM. IN CURVE (3), $\Delta f''$ IS NEGLECTED, IN CURVES (2) AND (1) IT HAS BEEN INCLUDED FOR VALUES OF SIN θ/λ EQUAL TO 0 AND 1 Å^{-1} RESPECTIVELY. AFTER R.W. JAMES (25) PAGE 152. FIGURE 53.

the Thomas-Fermi model to obtain f_0. This particular numerical value is selected because it would correspond to the approximate Bragg angle for diffraction from the (100) planes, should they exist in the TiM phases. We may then write

$$F(100)F(100)^* = [(f_0 + \Delta f_k')_M - (f_0 + \Delta f_k')_{Ti}]^2 + [(\Delta f_k'')_M - (\Delta f_k'')_{Ti}]^2 \quad .$$

Table IX gives the calculated values of F(100) for radiation varying in wavelength from chromium to molybdenum characteristic Kα. From these data alone chromium Kα would appear to be a good selection for a target element and this was indeed used by Philips and Beck (23). It is necessary, however, to examine in closer detail the expression for the calculated intensity of a Debye-Scherrer powder diffraction line bearing in mind the geometry of the experiment which we shall use, figure 20. We write a well known formula for the case of polarized incident radiation:

$$I(hk\ell) = I_0\left[\frac{e^2}{mc^2}\right]^2 P(\theta,\theta_M)L(\theta)\frac{F(hk\ell)F(hk\ell)^*}{16\pi r\ Vc^2}\ p\lambda^3\ dV\ A(\mu r,\theta)D.$$

The symbols are defined:

I_0 = Intensity of the incident beam

$I(hk\ell)$ = Calculated intensity of diffracted beam

e^2/mc^2 = Classical radius of the electron

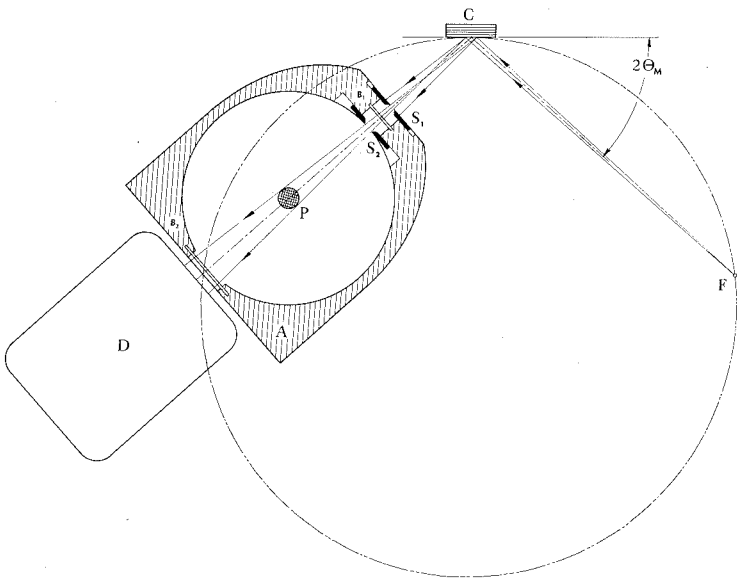

FIG. 20. THE EXPERIMENTAL ARRANGEMENT OF THE POWDER DIFFRACTION EXPERIMENT. A, THE DIFFRACTION CHAMBER; B_1 AND B_2, VACUUM SEALS; C, MONOCHROMATOR CRYSTAL; D, THE DETECTOR; F, FOCAL SPOT OF THE X-RAY TUBE; P, POWDER ROD SPECIMEN; S_1 AND S_2 ARE DEFINING AND LIMITING SLITS.

θ = Bragg angle for constructive interference from the plane (hkℓ).

θ_M = Bragg angle for the monochromator crystal

$P(\theta,\theta_M)$ = Polarization factor = $\dfrac{1 + \cos^2 2\theta_M \cos^2 2\theta}{1 + \cos^2 2\theta_M}$

$L(\theta)$ = Lorentz factor = $(\sin^2\theta\cos\theta)^{-1}$

r = Radius of the diffraction chamber

Vc = Volume of the unit cell

λ = Characteristic wavelength

p = Multiplicity factor

dV = Volume of specimen irradiated

$A(\mu r,\theta)$ = Absorption correction for powder rod

D = Temperature factor = exp.(-2M)

For a given (hkℓ) the observed intensity is influenced strongly by the Lorentz and polarization functions which are monatonic in nature. The effect of a short wavelength radiation such as molybdenum is to increase the magnitude of these contributions to the intensity expression, over that to be expected for chromium radiation, by a factor of about 3. The attractiveness of molybdenum Kα for this particular experiment is now apparent. A serious consideration remains and this presents itself in the λ^3 term of the intensity expression. It then becomes clear that a desirable feature of the diffraction chamber for this experiment is that it be evacuated

to reduce air scatter if short wavelength radiation is to be used. The long air path between the source and camera is another important factor which favors more energetic characteristic radiation.

THE DIFFRACTION EXPERIMENT

The experimental arrangement consisted of a commercial spectrometer based on the Bragg-Brentano focusing principle (26,27) and a specially constructed 72.0 mm diffraction chamber which was deployed in a manner shown schematically in figure 20. The line focus of the X-ray tube, which is normal to the focusing circle, is used as a source and is parallel to the powder rod at the center of the diffraction chamber. The primary beam was limited to 1° of divergence in the plane of the focusing circle, vertical divergence being somewhat restricted by a single Soller slit which was part of the spectrometer. Flat plate monochromator crystals were placed on the periphery of the focusing circle, in the position normally occupied by the powder block specimen. Reflecting planes were parallel to the ground surface. A lithium fluoride plate was used with molybdenum Kα, diffraction from (200); and the $(10\bar{1}1)$ planes of quartz were used to select characteristic copper Kα.

The diffraction experiment is shown in figure 21 and details of construction of the diffraction chamber are displayed in figure 22. The divergent beam of X-rays was defined and limited by two pair of adjustable slits built into the camera, S_1 and S_2. The second slit system can be seen from the inside of the camera. Scattering of X-rays by air was reduced by evacuating the diffraction chamber during the experiment. A vacuum of at least 25 microns was maintained.

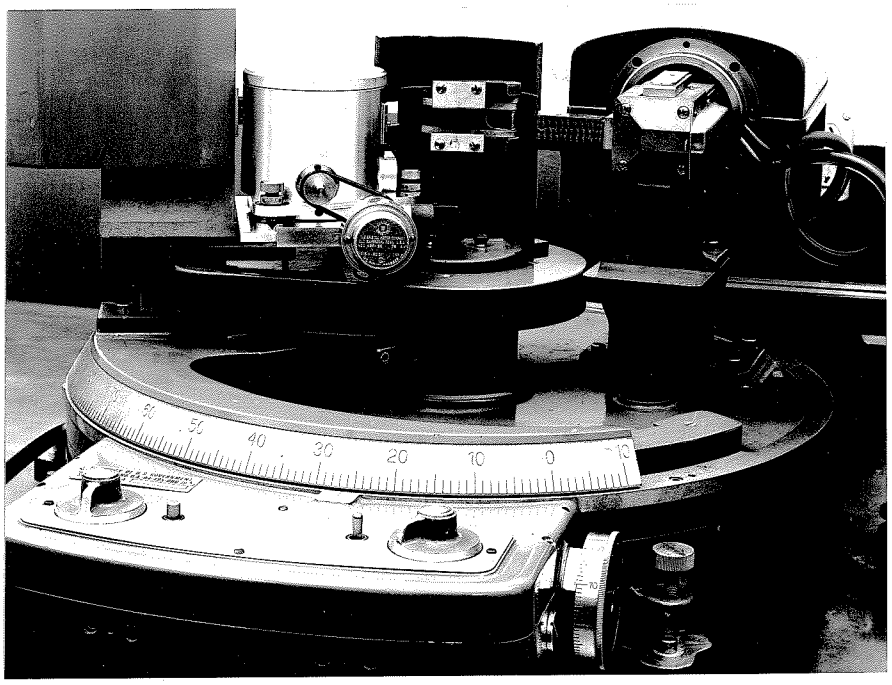

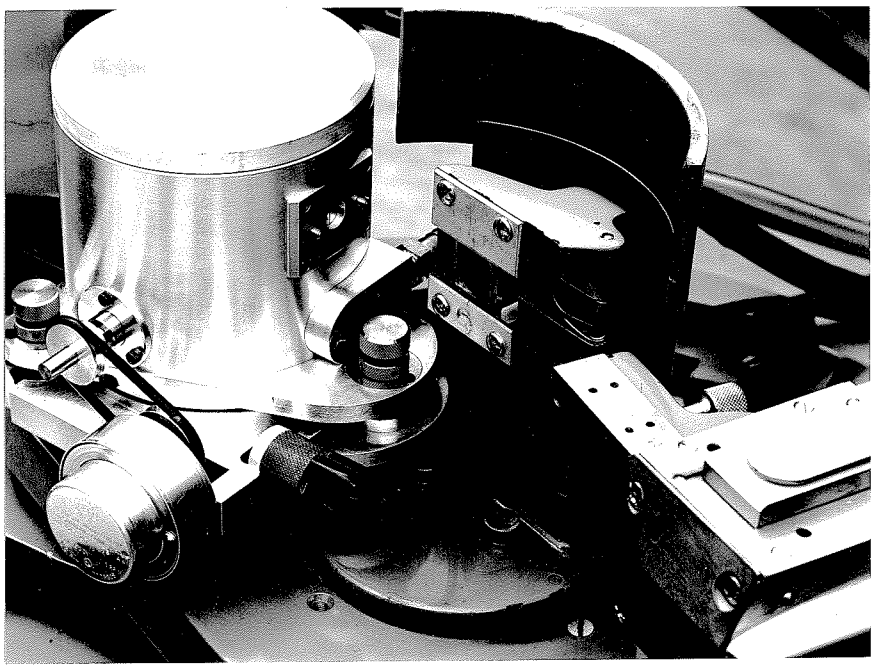

Fig. 21ab.--The X-ray diffraction experiment. Relationship of diffraction chamber to the spectrometer.

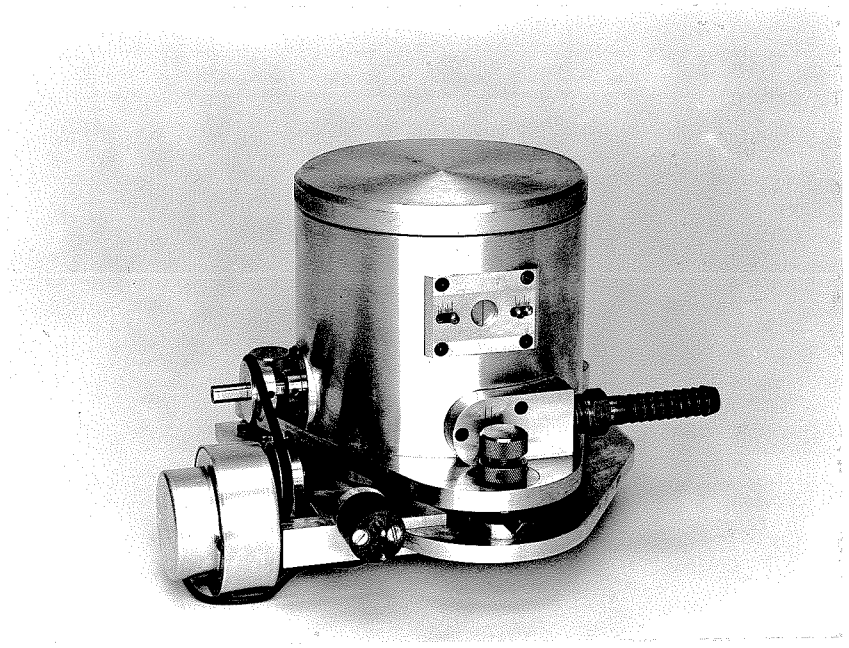

(a)

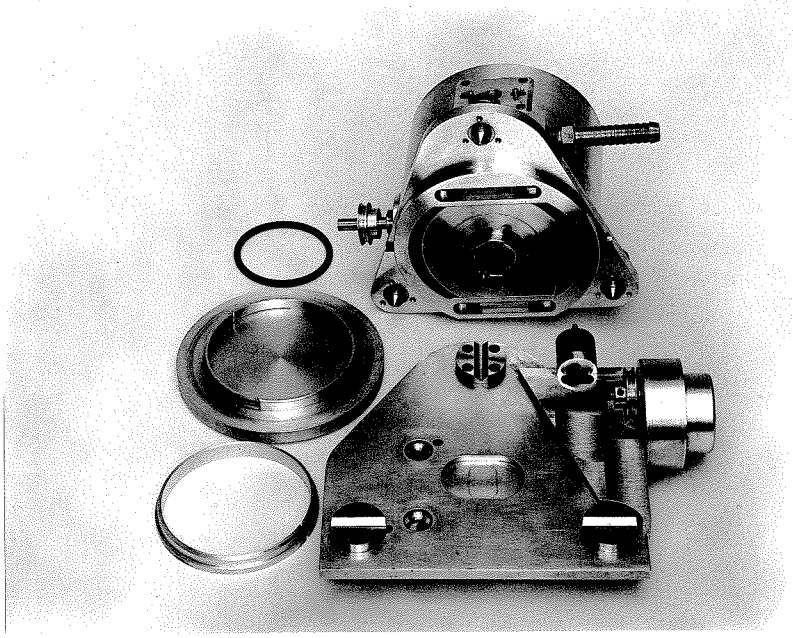

(b)

Fig. 22abcd.--Details of construction, the diffraction chamber

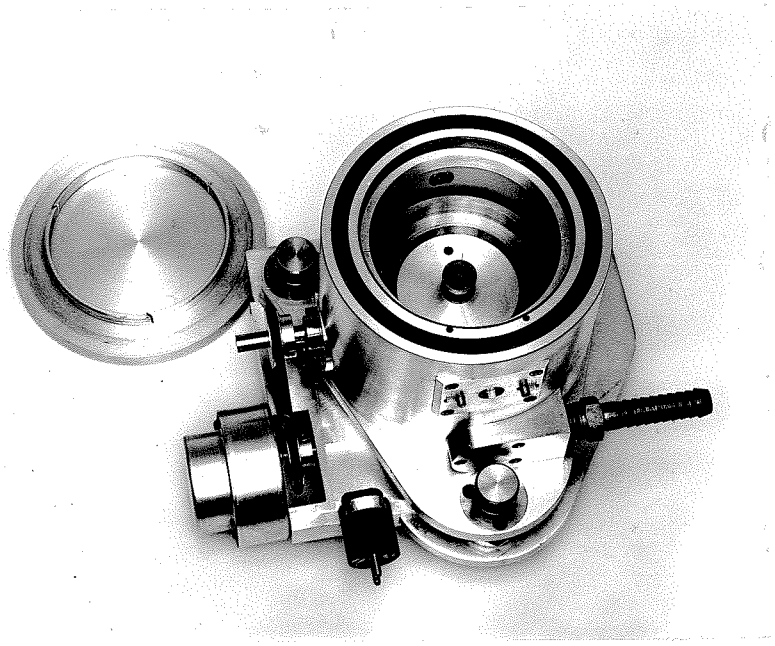

(c)

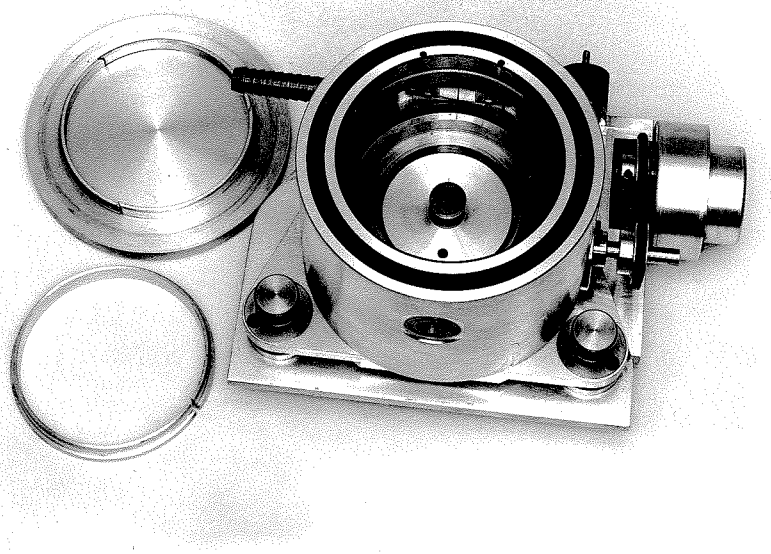

(d)

The spectrometer detector was employed to select and orient monochromator crystals. Final adjustments of the diffraction chamber relative to the beam were made by photographic methods; the mechanical devices for this purpose are those conventionally used in instruments and may be viewed in figure 22.

RESULTS

Evidence for the cesium chloride type crystal structure in TiFe is given in figure 23a which is a powder diffraction pattern made with molybdenum Kα radiation. The exposure time was 120 hours and a space current of 20 ma was used. Four weak maxima were observed. Calculated intensities are presented in Table X, these were computed with the simplified expression:

$$I(hk\ell) = \text{constant } P(\theta,\theta_M)L(\theta)F(hk\ell)F(hk\ell)^* \text{ p } A(\mu r,\theta)$$

The values of $A(\mu r,\theta)$ which were used correspond to $\mu r = 2.2$ for the powder rod specimen irradiated with MoKα. A similar diffraction photograph was obtained for TiCo, four weak reflections being recorded. To obtain evidence for TiNi the spectrometer was adjusted to receive monochromated CuKα from a quartz plate. One of the resulting photographs, figure 23b, represents an exposure time of 72 hours and space current of 15 ma. The resulting diffraction maxima indicated that two equilibrium phases were present, TiNi and Ti_2Ni. This observation is in agreement with the metallography since none of the homogenized ingots used for powder specimens were entirely one phase. Indexing of the Ti_2Ni spectrum is taken from reference 22. We observe that the (100) of TiNi is very definitely present and that the (210) of TiNi, which could be

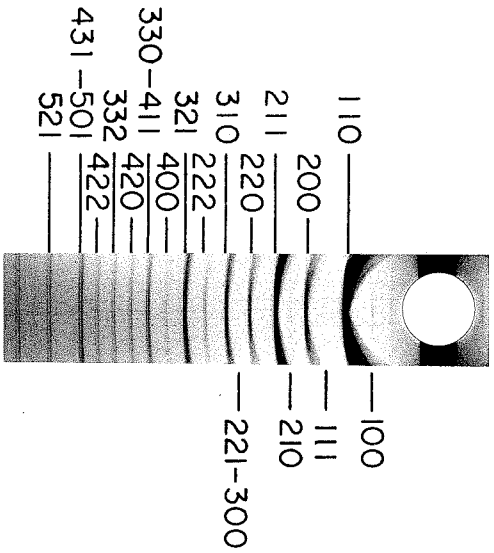

Ti Fe (a)

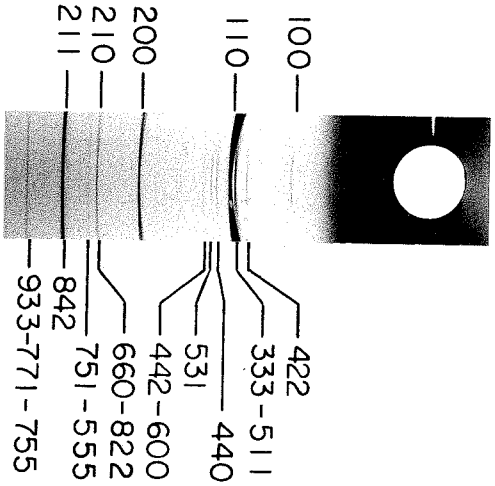

Ti Ni (b)

Ti_2Ni

FIG. 23a,b. POWDER DIFFRACTION PHOTOGRAPHS. SPECTRUM OF TiFe MADE WITH MoKα, 120 HOURS, 20 ma, FIG. 23a. SPECTRUM OF TiNi MADE WITH CuKα, 72 HOURS, 15 ma, FIGURE 23b.

present even if the (111) were not observed, is at a Bragg angle which permits superposition with the (660) and (822) reflections of Ti_2Ni. Although we have observed only one diffraction maxima which may be associated unequivocally with long range order in TiNi this evidence is strong since neither of the adjacent phases, Ti_2Ni and $TiNi_3$, in the constitution diagram produce constructive interference which is recorded at the same Bragg angle as the (100) of TiNi. Thus we have demonstrated, by X-ray powder diffraction experiments, that TiFe, TiCo, and TiNi are cesium chloride B2 type crystal structures.

Table IX. Variation of F(100) with Wavelength for the TiM Phases

Radiation		F(100) TiFe	TiCo	TiNi
Cr Kα	2.2909 Å	4.76	5.63	6.49
Co Kα	1.7902 Å	2.18	2.90	3.99
Cu Kα	1.5418 Å	2.17	2.17	2.29
Mo Kα	0.7107 Å	3.46	4.37	5.35

Table X. X-Ray Powder Diffraction Data for TiFe made with a 72.0 mm camera. Exposure time 120 hours. Monochromated Mo Kα radiation, 20 ma.

hkl	$\sin^2\theta$ obs.	$\sin^2\theta$ calc.	Relative Intensity* $I_{obs.}$	Relative Intensity* $I_{calc.}$
100 α	.0133	.0142	W	365
110 α	.0273	.0284	VS	22769
111 α	.0421	.0426	WW	86
200 α	.0578	.0568	MS	4262
210 α	.0706	.0710	VW	138
211 α	.0852	.0852	S	9458
220 α	.1144	.1136	M	2999
300 α	.1280	.1278	VW	18
221 α				73
310 α_1	.1424	.1420	M	2730
311 α_1		.1562	A	38

*Observed intensities are recorded in the following nomenclature: VS, very strong; S, strong; MS, medium strong; M, medium; WM, weak medium; W, weak; VW, very weak; VVW, very very weak; and A indicated no reflection observed.

PART III

THE CONFORMAL PHASE $TiPt_8$

INTRODUCTION

The manner in which the crystal structure of $TiAu_4$ was determined is an illustration of how one may utilize the most elementary observations and considerations to arrive at a trial structure which is very close to the actual crystal structure. This is not the usual procedure which is followed in determination of the electron density in a periodic space lattice. The method of analysis which we have set forth does work in the case already described because of the relationship which exists between the space lattices of the terminal solid solutions, the pseudo cell, and $TiAu_4$. We shall now apply these same methods to a novel crystal structure which was found during an investigation of some titanium-platinum alloys.

An exploratory study was performed with alloys in region of the partial constitution diagram $TiPt_3$-Pt. Those compositions which were investigated are 2, 4, 6, 8, 9, 10, 12, 16, 20 and 25 atomic percent titanium. The electric-arc melted ingots were homogenized at 1000°C and equilibrated at 400°C. X-ray diffraction experiments indicated the presence of a limited region of solid solubility of titanium in face-centered cubic platinum. After a heat-treatment at 400°C for 30 days the maximum solubility of titanium in alpha solid solutions is between 4 and 6 atomic percent. We see that here, as in the titanium-gold system, the addition of titanium to face-centered cubic platinum results in a decrease in the lattice

parameter of the parent phase. The existence of $TiPt_3$, an ordered $AuCu_3$ type structure, which was reported by Wallbaum (28) has been confirmed by this investigation. Another intermediate phase was found at approximately 10 atomic percent titanium and identified as $TiPt_8$. We shall now describe this crystal structure.

A few remarks may be in order so that the reader will understand the nature of the difficulties that are presented by this problem. The X-ray diffraction spectrum, like that of $TiAu_4$, consists of very strong and very weak lines. However, in the case of $TiPt_8$ the intensity ratio of strong to weak maxima is much greater. The Debye-Scherrer powder diffraction photograph, when made with unmonochromated radiation, is not desirable for the study of these weak maxima. One would like to reduce the background intensity of the film which is due in part to the Bremsstrahlung. This suggests an experimental arrangement in which the primary beam is monochromated, and if possible focused to an image on the film. The author is indeed grateful to Dr. Sten Sampson of the Crellin Chemistry Laboratory for suggesting the use of the Guinier type camera for this problem. It was through Dr. Sampson's efforts that a sample of $TiPt_8$ was transmitted to Dr. Georg Lundgren of the Department of Physical and Inorganic Chemistry, University of Stockholm,and X-ray diffraction photographs of this alloy were made with the apparatus shown schematically in figure 24. While it may very well be that this crystal structure could have been determined with the

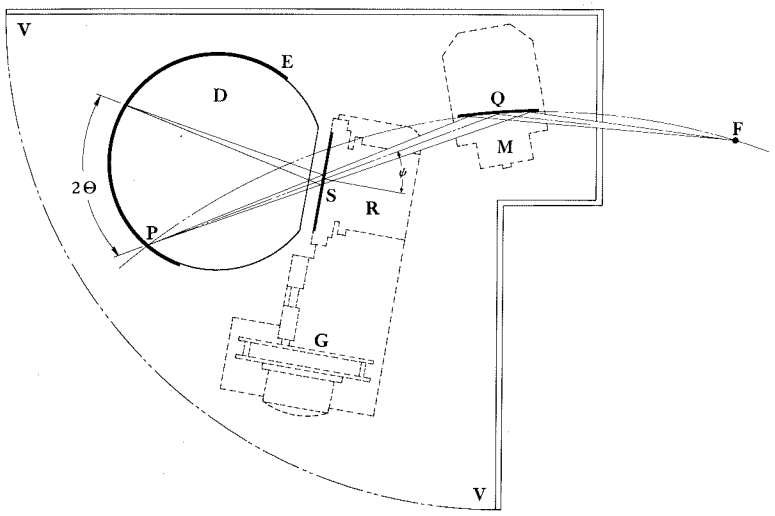

FIG. 24: THE EXPERIMENTAL ARRANGEMENT FOR THE GUINIER TYPE CAMERA. THE SCHEMATIC REPRESENTATION SHOWS: D, THE DIFFRACTION CHAMBER; E, THE PHOTOGRAPHIC FILM; F, THE FOCAL SPOT OF THE X-RAY TUBE; G, THE MOTOR DRIVE; M, CRYSTAL MONOCHROMATOR HOLDER AND ADJUSTMENTS; P, IMAGE OF THE LINE FOCUS; R, DEVICE FOR ROTATING THE SPECIMEN; AND S IS THE POWDER DIFFRACTION SPECIMEN.

usual Debye-Scherrer powder diffraction experiment, the value of the Guinier camera for this type of problem, and indeed many others, cannot be overemphasized. Having obtained such X-ray photographs through the kindness of Dr. Sampson and Dr. Lundgren there was the problem of determining the intensity formula for such an experiment. The literature does contain an approximate expression which is due to a private communication from Professor Hägg (29). Since the degree of approximation was not discussed in this paper by Berger (29) the present author felt obligated to write and use a complete relative intensity expression. Thus we shall first discuss the factors which enter into the intensity expression and then proceed to the crystal structure determination itself.

THE INTENSITY EXPRESSION

Many features of the apparatus which are shown schematically in figure 24 have been described and discussed by A. Guinier (30). An intensity expression for a camera disposed in this asymmetric arrangement has not been derived in the literature. Since the purpose of this investigation is to determine a new atomic motif it is quite relevant and indeed necessary that we write the complete intensity expression and set forth the assumptions on which it is based.

Let us start with an expression which is given by James (25). The power which is diffracted into a short segment of a powder diffraction halo is given by formula 2.48 which follows:

$$\frac{P}{I_o} = \frac{p(hk\ell)b}{8\pi r \sin\theta} QV ,$$

where

P = Power reflected into a segment of diffraction halo.

b = Length of halo segment.

I_o = Intensity of incident beam.

r = Length of path of the diffracted beam within the camera.

θ = Bragg angle for constructive interference.

V_p = Total volume of the powder irradiated by the primary beam.

$P(hk\ell)$ = Multiplicity factor of the form $hk\ell$.

Following the convention which is found in the literature we write:

$$Q = \frac{|F(hk\ell)|^2 N^2}{\sin 2\theta} \left[\frac{e^2}{mc^2}\right]^2 \lambda^3 \left[\frac{1 + \cos^2 2\theta}{2}\right]$$

in which

$F(hk\ell)$ = Structure factor of plane $(hk\ell)$

N = Number of atoms per unit volume

$\frac{e^2}{mc^2}$ = Classical radius of the electron.

λ = Wavelength of the light

$\frac{1+\cos^2 2\theta}{2}$ = Polarization factor.

Since our apparatus does include a quartz crystal monochromator we shall replace Q by Q_M. This requires that a different expression be used for the polarization factor. If θ_M is the Bragg angle for constructive interference for the monochromator crystal we have

$$Q_M = \frac{|F(hk\ell)|^2 N^2}{\sin 2\theta} \left[\frac{e^2}{mc^2}\right]^2 \lambda^3 \left[\frac{1 + \cos^2 2\theta \cos^2 2\theta_M}{1 + \cos^2 2\theta_M}\right]$$

The only assumption which has been made thus far is that an isotropic distribution of grains does exist. It is ex-

tremely important that this requirement is fulfilled and we shall comment on this matter later. We now write an expression for the intensity of the maxima $(hk\ell)$,

$$I(hk\ell) = \text{constant}\ \frac{|F(hk\ell)|^2 p(hk\ell)}{r \sin^2\theta \cos\theta}\ \frac{1+\cos^2 2\theta \cos^2 2\theta_M}{1+\cos^2 2\theta_M}\ A_s A_c A_f$$

The three quantities which remain to be determined are effects due to absorption. Let us define some quantities which are necessary for this purpose.

A_s = Attenuation of the primary beam S_o by the specimen.

A_c = Attenuation of the diffracted beam S by the air within the camera enclose if it is not evacuated.

A_f = Absorption of the diffracted beam S by the film emulsion.

μ_s = Linear absorption coefficient of the specimen.

μ_c = Linear absorption coefficient of the atmosphere within the camera enclose.

μ_f = Linear absorption coefficient of a single emulsion of the film.

t_s = Specimen thickness.

t_f = Film emulsion thickness.

R = Radius of the diffraction chamber.

r = $2R\cos\eta$

η = $2\theta - \psi$

ψ = Angle between S_o and the normal to the surface of the specimen.

To determine A_s we assume that $\vec{S}_o$ is a parallel bundle of rays, an assumption that is not unreasonable since the angle of divergence in the plane of the focusing circle is small. A portion of the specimen is depicted in figure 25; the z axis is normal to the plane of the illustration. The lengths of the specimen in the y and z directions are taken to be unity. At some distance $x = x_1$ the path of the incident radiation to an infinitesimal of volume is $x_1 \sec\psi$ and the length of the path from x_1 to the free surface is $(t - x_1)\sec\eta$. Integration of the usual exponential law of attenuation throughout the entire volume of the specimen leads to the following expression:

$$A_s = \frac{1}{\mu_s\left[\frac{\cos\psi}{\cos\eta} - 1\right]} \left[\exp(-\mu_s t_s \sec\psi) - \exp(-\mu_s t_s \sec\eta)\right]$$

The diffracted beam $\vec{S}$ may suffer an exponential loss in intensity if the camera is not evacuated. This will be a function of the Bragg angle as indicated:

$$A_c = \exp(-\mu_c r) = \exp(-\mu_c 2R\cos\eta)$$

Since the diffracted beam does not enter the film radially we must include an absorption factor for this effect. The exact form of this quantity will depend on the geometry of the diffraction experiment as well as technique. In a

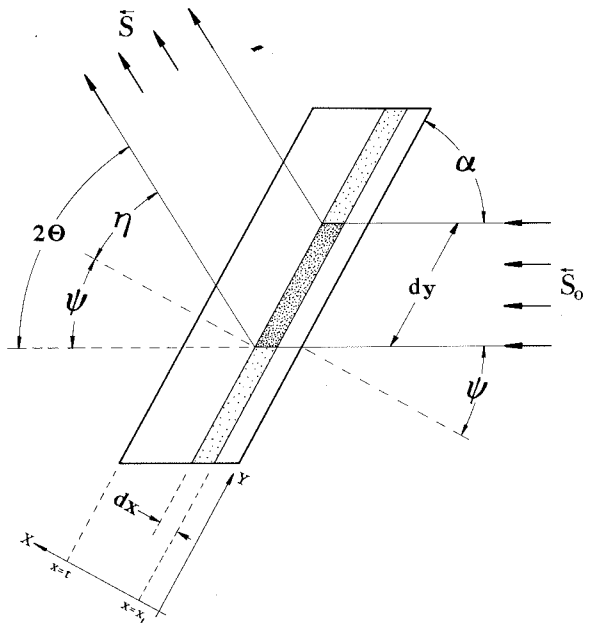

FIG. 25. GEOMETRY OF THE CORRECTION FOR ABSORPTION WITHIN THE SPECIMEN.

Debye-Scherrer type camera one usually employs double emulsion X-ray film. Here the diffraction maxima enter the film radially. It is evident that for an asymmetric camera there are disadvantages which may result if double emulsion film is used since the two images of the diffraction maxima may not superimpose and thus we lose one of the advantages of a focusing geometry. For this reason it is convenient, when using the Guinier type camera, to remove the film emulsion which is most remote from the specimen after the X-ray film is developed. A single emulsion recording of the data such as we have described does not require absorption constants for the film base and we may write:

$$A_f = [1 - \exp(-\mu_f t_f \sec\eta)]$$

The dimensionless parameter $\mu_s t_s$ was determined from the specimen of $TiPt_8$ which was used in Sweden in the Guinier camera. The author obtained CuKα radiation by use of a quartz plate and measured the attenuation of the beam with a detector. The specimen was oriented in several directions within its own plane and an average value of $\mu_s t_s$ obtained. This is quite necessary since the specimen is rotated during the length of time required for an exposure. It was not known if the camera enclosure VV was evacuated when the X-ray film was exposed. When CuKα radiation is used this correction is relatively small. An estimate of the magnitude of this function

may be obtained from data given by Guinier (31). In this reference the transmission factor for CuKα in a 10 cm air path is 0.89. The last dimensionless constant $\mu_f t_f$ was taken from Berger (29) since it was known that Eastman Kodak film was used. Values of constants for the experiment are as follows:

$$R = 40 \text{ mm}$$

$$\gamma = 29°$$

$$\mu_s t_s = 1.5$$

$$\mu_c = 0.011 \text{ cm}^{-1}$$

$$\mu_f t_f = 0.13$$

THE CRYSTAL STRUCTURE OF $TiPt_8$

The methods we shall employ to determine the crystal structure of $TiPt_8$ are in principle the same as were used to establish the atomic motif of $TiAu_4$. Once again we are motivated by an X-ray diffraction pattern which consists of either strong or very weak reflections. We observe that the more intense reflections could be explained, both as to position and intensity, by assuming the existence of a pseudo space lattice of face-centered tetragonal symmetry and a unit cell containing four statistical atoms. It is evident from the intensities of the pseudo tetragonal cell that the atoms must lie in nets which are very nearly or in fact actually at the distances $z = 0$, and $z = 1/2$. This assumption was demonstrated to be quite reasonable in the case of $TiAu_4$ by the single crystal and powder diffraction data. It is these observations which allow us to reduce our problem to that of a 2-dimensional space. Powder diffraction data which is given in Table XI was indexed with a Hull Davey chart. The (00ℓ) reflections of the pseudo cell were assumed to be invariant to a transformation. The space lattice of the pseudo cell is related to the crystallographic lattice of $TiPt_8$ by the relationship:

$$\begin{pmatrix} a_3 \\ b_3 \\ c_3 \end{pmatrix} = \begin{pmatrix} \gamma_{11} & \gamma_{12} & 0 \\ \gamma_{21} & \gamma_{22} & 0 \\ 0 & 0 & \gamma_{33} \end{pmatrix} \begin{pmatrix} a_p \\ b_p \\ c_p \end{pmatrix}$$

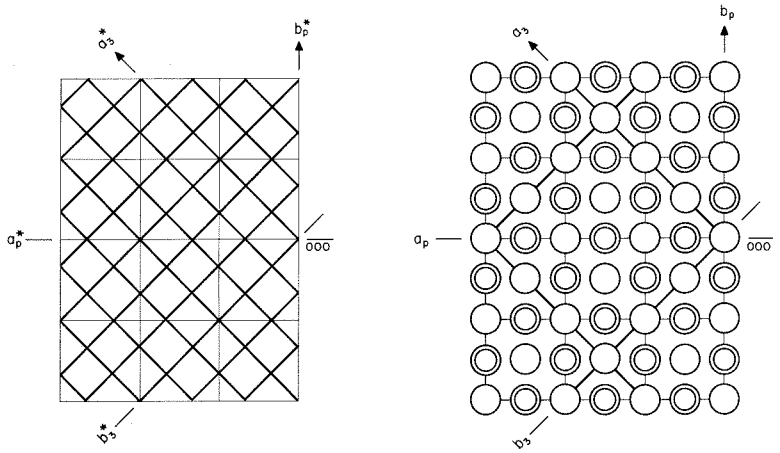

(a) (b)

FIG. 26. ORIENTATION RELATIONSHIPS OF THE INTERMEDIATE PHASE $TiPt_8$ AND A PSEUDO TETRAGONAL LATTICE IN (a) RECIPROCAL SPACE AND (b) OBJECT SPACE.

where

$$\gamma_{11} = \gamma_{21} = \gamma_{12} = -\gamma_{22} = 3/2 \text{ and } \gamma_{33} = 1.$$

The lattice parameters were determined by the method due to Cohen (7). Data were obtained from a 143.2 mm Debye-Scherrer camera in which CrKα was used. Maxima from the 600 $K\alpha_1$, 332 $K\alpha_1 K\alpha_2$, 631 $K\alpha_1 K\alpha_2$, and 303 $K\alpha_1 K\alpha_2$ reflections yield the following lattice constants:

$$a_3 = b_3 = 8.312 \text{ Å}, \quad c_3 = 3.897 \text{ Å}, \quad c_3/a_3 = 0.469 \quad .$$

The indexing of Table XI reveals that only one systematic extinction does exist: $(hk\ell)$ present only if $h + k + \ell = 2n$. This implies that we are dealing with a body-centered tetragonal space lattice. Space groups which become possible on the basis of this information are:

$$D_{4h}^{17} - I4/mmm, \; D_{2d}^{11} - I\bar{4}2m, \; C_{4v}^{9} - I4mm, \; D_{4}^{9} - I422,$$

$$C_{4h}^{5} - I4/m, \; S_{4}^{2} - I\bar{4}, \text{ and } C_{4}^{5} - I4.$$

At this stage of the analysis we admit space groups which belong to Laue symmetry groups 4/m and 4/mmm.

The atomic population of the new unit cell may be obtained by evaluating the matrix just written since its geometrical interpretation is a volume. This leads to the conclusion that $V_3 = 9/2\ V_p = 18$ atoms. Since there are two lattice

points per unit cell we arrive at $TiPt_8$ (11.1 atomic percent titanium) as the stoichiometric composition of the first platinum-rich intermediate phase. This is in agreement with our visual estimate of the position of this phase which was 10 atomic percent.

Let us now seek a trial structure. We write a relationship between the pseudo cell and the unit cell of $TiPt_8$ in reciprocal space:

$$\begin{pmatrix} a_3^* \\ b_3^* \\ c_3^* \end{pmatrix} = \begin{pmatrix} \beta_{11} & \beta_{12} & 0 \\ \beta_{21} & \beta_{22} & 0 \\ 0 & 0 & \beta_{33} \end{pmatrix} \begin{pmatrix} a_p^* \\ b_p^* \\ c_p^* \end{pmatrix}$$

where the matrix coefficients are written

$$\beta_{11} = \beta_{12} = \beta_{21} = -\beta_{22} = 1/3 \quad \text{and} \quad \beta_{33} = 1 \ .$$

With these relationships we may now relate the position of the j^{th} atom in the pseudo cell, which resides at $(x_p, y_p, z_p)_j$, to its coordinates in the correct unit cell which we designate $(x_3, y_3 z_3)_j$. The region of space on which we operate is shown in figure 26b. We now list the results of the transformation and indicate negative direction with a bar.

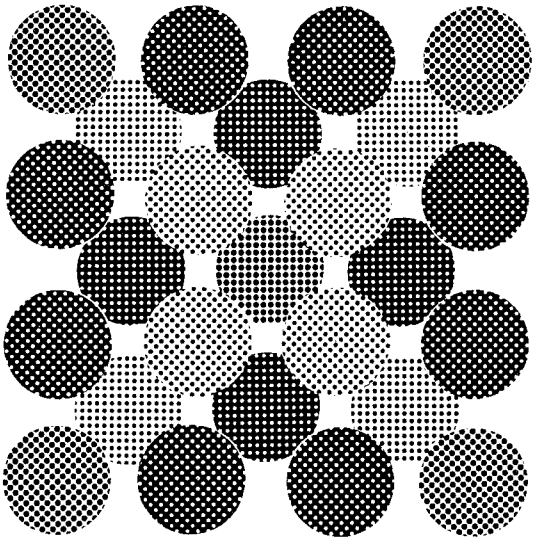

FIG. 27. THE CRYSTAL STRUCTURE OF $TiPt_8$. ATOMS WHICH ARE FULL REPRESENT THE NET $z=0$, OTHERS ARE IN THE NET $z=1/2$. LIGHT ATOMS ARE IN (h), MEDIUM INTENSITY ATOMS IN (a), AND THE DARKEST SHADING REFERS TO ATOMS IN (i) OF D_{4h}^{17}.

j	x_p, y_p, z_p	x_3, y_3, z_3	D_{4h}^{17}
1	0,0,0	0,0,0	a
2	3,0,0	1,1,0	a
3	3/2,3/2,0	1,0,0	a
4	3/2,$\overline{3/2}$,0	0,1,0	a
5	3/2,0,1/2	1/2,1/2,1/2	a
6	1/2,1/2,0	1/3,0,0	i
7	1/2,$\overline{1/2}$,0	0,1/3,0	i
8	1,1,0	2/3,0,0	i
9	1,$\overline{1}$,0	0,2/3,0	i
10	1,$\overline{1/2}$,1/2	1/6,1/2,1/2	i
11	1,1/2,1/2	1/2,1/6,1/2	i
12	2,1/2,1/2	5/6,1/2,1/2	i
13	2,$\overline{1/2}$,1/2	1/2,5/6,1/2	i
14	1,0,0	1/3,1/3,0	h
15	3/2,1/2,0	2/3,1/3,0	h
16	3/2,$\overline{1/2}$,0	1/3,2/3,0	h
17	2,0,0	2/3,2/3,0	h
18	2,1,0	1,1/3,0	h
19	2,$\overline{1}$,0	1/3,1,0	h
20	5/2,1/2,0	1,2/3,0	h
21	5/2,$\overline{1/2}$,0	2/3,1,0	h
22	1/2,0,1/2	1/6,1/6,1/2	h
23	3/2,1,1/2	5/6,1/6,1/2	h
24	3/2,$\overline{1}$,1/2	1/6,5/6,1/2	h
25	5/2,0,1/2	5/6,5/6,1/2	h

The results of the transformation can now be written with the notation of the International Tables for X-Ray Crystallography (10); considering the ensemble to be in space group D_{4h}^{17} we have,

0,0,0; 1/2,1/2,1/2 +

2 Ti in (a): 000

8 Pt in (h): x,x,0; $\bar{x}$,$\bar{x}$,0; x,$\bar{x}$,0; $\bar{x}$,x,0 with $x_1^{(o)} = 1/3$.

8 Pt in (i): x,0,0; $\bar{x}$,0,0; 0,x,0; o,$\bar{x}$,0 with $x_2^{(o)} = 1/3$.

The space group possibilities are quite limited. In D_{4h}^{17} for example, the 16-fold positions n, m, ℓ, and k can be ruled out because of packing considerations. In effect what we are saying is that the actual disposition of atoms requires only small perturbations of the trial structure or ideal atomic positions, and within the symmetry requirements of this space group the use of 16-fold positions is not compatible with these concepts. The description we have written is valid for D_{4h}^{17} or D_4^9; we have chosen the space group of highest symmetry. The introduction of either one or two z parameters, in addition to x_1 and x_2, requires that the space group be either D_{2d}^{11} or C_{4v}^9. We have already commented on the evidence which is present in the strong reflections and suggest that the atoms lie in nets at z = 0 and 1/2.

For this reason we shall confine our attention, at the moment, to the space group of highest symmetry in Laue symmetry group 4/mmm. The Datatron which is manufactured by the Electrodata Corporation was used to calculate structure factors in x_1, x_2 space. Two different intervals of this space were investigated as the region of interest narrowed. The increments at which each structure factor was calculated is given in square brackets.

(i) x_1: 0.324 ..... [0.002] 0.344
x_2: 0.324 ..... [0.002] 0.344

(ii) x_1: 0.324 ..... [0.001] 0.336
x_2: 0.324 ..... [0.001] 0.336

The best fit to the observed relative intensities, using space group D_{4h}^{17}, was obtained with the following disposition of atoms:

0,0,0; 1/2,1/2,1/2 +

2 Ti in (a)
2 Pt in (h) with $x_1^{(ii)} = 0.333$
2 Pt in (i) with $x_2^{(ii)} = 0.327$.

DISCUSSION

While the agreement between observed and calculated intensities is satisfactory the crystal structure determination cannot be considered complete. It is possible to find a motif of atoms belonging to the Laue symmetry class 4/m which would also explain the intensity data. Thus if we were to use space group C_{4h}^5, there would be four possible parameters in the x-y plane. Following our previous discussion the admission of two and three z parameters would require the symmetry of S_4^2 and C_4^5. One might resolve some of these questions with single crystal diffraction experiments. The author made many attempts to obtain a single crystal of $TiPt_8$ but was not successful. Specimens with dimensions as small as 0.02 mm gave powder diffraction halos due to the characteristic Lα radiation of the wolfram target. Thus, while we are assured an isotropic distribution of grains for the powder diffraction experiment, we lack valuable single crystal evidence concerning the symmetry. One might attempt to make a single crystal of $TiPt_8$ in the manner which was used for $TiAu_4$. Here we require a knowledge of the phase diagram, which does not yet exist.

Table XI. X-Ray Powder Diffraction for the Intermediate Phase $TiPt_8$. Monochromated Copper Characteristic Radiation.

hkl		$Sin^2\theta$ Observed	$Sin^2\theta$ Calculated	Relative Intensities Observed	Relative Intensities Calculated
110	α	.0174	.0172	VW	6.32
200	α	.0346	.0345	W	10.16
101	α	.0480	.0478	W	9.02
220	α	.0691	.0690	VW	5.00
211	α	.0827	.0823	W	10.91
310	α	.0869	.0862	VW	3.66
301	α	.1171	.1168	VVS	331.45
400	α	.1388	.1379	VVVW	0.39
321	α	.1521	.1513	VW	6.04
330	α	.1552	.1552	S	111.25
002	α	.1591	.1568	M	55.97
420	α		.1724	A	1.15
112	α		.1740	A	1.16
411	α		.1857	A	0.96
202	α		.1913	VVW	2.14
510	α	.2252	.2241	VVW	2.10
222	α	.2263	.2258	VVW	2.11
312	α	.2438	.2430	VVW	1.84
501	α	.2519	.2547	VVW	2.22
440	α		.2758	A	0.04
521	α		.2892	VW	4.21
530	α	.2960	.2931	VVW	1.93
402	α_1		.2947	A	0.31
600	α_1	.3104	.3103	M	46.66
332	α_1	.3127	.3120	S	90.22
422	α_1	.3302	.3292	A	1.01
620	α_1		.3448	A	1.19
611	α_1	.3600	.3576	VVW	1.35
103	α_1		.3614	A	0.59
512	α_1	.3830	.3809	VVW	2.36
213	α_1	.3933	.3959	VVW	1.61
631	α_1	.4266	.4271	VS	144.98
303	α_1	.4297	.4304	S	105.60
710	α_1		.4310	A	0.07

Table XI (continued)

hkℓ		$\sin^2\theta$ Observed	$\sin^2\theta$ Calculated	Relative Intensities Observed	Relative Intensities Calculated
550	α_1		.4310	A	1.50
442	α_1		.4326	A	0.10
640	α_1		.4482	A	0.41
701	α_1		.4616	A	0.07
323	α_1	.4664	.4649	S	2.81
602	α_1	.4664	.4671		104.81

Observed intensities are designated as follows: VVS, very very strong; VS, very strong; S, strong; M, medium; W, weak; VW, very weak; VVW; very very weak; and VVVW, very very very weak. The letter A indicates that a reflection was not observed for the corresponding (hkℓ).

CONCLUSIONS

The solid state modes of decomposition of a face-centered cubic solid solution represents one of the most engrossing fields of research in physical metallurgy. The advent of X-ray diffraction theory and techniques gave impetus to the study of this subject on an atomic scale. Kirchner (32) studied the lattice parameters of the continuous series of solid solutions in copper-gold alloys. This work was done during the years 1920-21. It was not until 1925 that Johansson and Linde (33) published the crystal structures of CuAu and $CuAu_3$. It then became apparent that at least two modes of decomposition of the face-centered cubic lattice, with a random distribution of atoms, was possible. In the case of CuAu the lattice was tetragonal, while for Cu_3Au it was found to be primitive cubic. A striking feature of both crystal structures was the simple geometrical relationships between the high temperature phase and the low temperature phases of stoichiometric composition. For many years these observations guided much of the thinking in the investigation of constitution diagrams which displayed extensive regions of alpha face-centered cubic solid solutions. One finds in the literature many examples of low temperature phases which are described as a "distorted CuAu type" or a "distorted Cu_3Au type" crystal structure. Very often the phase boundaries are poorly defined since the experimental

results are not in agreement with a 1:1 or 3:1 atomic composition ratio. It would seem that the concept of "ordering" and of definite composition ratio in such alloys crystallized the thinking with regard to the phase equilibria. Harker (16) determined the crystal of Ni_4W in the year 1944 and showed how this atomic motif was related to the tetragonal CuAu type crystal structure. Both space lattices are tetragonal, the differences being a function of the number and location of each species of atoms which are present. Hence the difference in stoichiometric ratio.

With the results of our present investigation we may extend our understanding of these phases. The crystal structure of $TiAu_4$ has been determined and is isomorphous with WNi_4. We have, however, found it necessary to change the ideal positional parameters. That is to say one must perturb the positions of atoms as deduced from the conformal transformation. In this respect there is a considerable difference between the crystal structure of $TiAu_4$ and isomorphs reported in the literature (16,17). A new atomic motif has been determined. This is the intermediate phase $TiPt_8$. Once again it has been found that a conformal transformation leads to a trial structure and that a perturbation of these atomic positions is required to obtain satisfactory agreement between calculated and observed intensity data. With the understanding of these "conformal phases," as well as others

which may exist, one may now turn to the great wealth of early experimental work and seek the true nature of the phase equilibria wherein modes of decomposition of the solid state have been poorly defined.

MATERIALS

The titanium metal used in this investigation was purchased from the New Jersey Zinc Co. It had been produced by the iodide reduction process. A typical chemical analysis of this material reported in weight percent by the vendor is as follows: manganese, 0.0065; iron, 0.0022; copper, 0.0015; and lead, 0.0042. Gold and platinum of chemical purity was furnished by Wildberg Brothers, San Francisco. The transition elements of iron, cobalt, and nickel were obtained from Johnson, Matthey and Co., Ltd., London.

EXPERIMENTAL PROCEDURES

Melting. Features and operational procedures for the electric arc melting apparatus which was used have been described in the literature by Schramm, Gordon, and Kaufmann (34). Charges weighed to the nearest milligram were melted in an atmosphere of helium. The ingots, approximately 8 gr in weight, were turned over and remelted; this procedure was repeated until homogeneity was achieved. Total weight losses were of the order of 0.1 pct.

Heat Treatment. Nichrome element furnaces were used up to 1000°C (1832°F); higher temperatures, to 1316°C (2400°F), were obtained with Globar element furnaces. Temperature control within $\pm$ 3°C was accomplished with Leeds and Northrup

Micromax controllers and recorders. To obtain a more uniform temperature distribution within these furnaces, ceramic and metal insert blocks were used as specimen holders; also, a deep vertical furnace was filled with refractory brick which had been bored to admit one specimen for heat treatment; temperature control for this furnace could be maintained at $\pm$ 1.5°C. Alloys placed in these horizontal and vertical furnaces were sealed in either Vycor or quartz ampoules which had been evacuated to 10^{-5} mm Hg or better. Vials containing specimens that were heated above 1000°C contained a pressure of helium sufficient to prevent the collapse of the container when at temperature. Alloy reaction at the higher temperatures was reduced by introducing molybdenum sheet liners into the quartz vials; in addition, alloys rich in titanium contained a getter of metallic zirconium. After the heat treating cycle had been completed, the vials were quenched in water and broken.

The induction heating furnace used for high temperature heat treatments, incipient melting observations, and melting point determinations was similar to the unit described by Schramm et al. (34). Design features allowed the specimen to be heated in vacuum or inert atmosphere and then quenched into a Silicone oil bath which was placed below the heating chamber. A simple mechanical device was used to protect the Pyrex optical pyrometer sight window from vapors when temperature readings were not being made. Various susceptors of

sintered wolfram and sheet molybdenum were used.

An optical pyrometer was calibrated for this particular experimental arrangement by observing the melting points of copper (1076, 1077, 1078°C), palladium (1546, 1560, 1573°C), platinum (1782, 1783, 1784°C), and rhodium (1937, 1938°C). Accepted values for the melting points of these elements (9) are: copper (1083°C), palladium (1554°C), platinum (1774°C), and rhodium (1966°C). All observations for copper, palladium, and platinum are given equal weight in deriving a linear calibration expression:

$$T_{corrected}\ (°F) = 0.9781\ T_{observed}\ (°F) + 54\ F$$

In a separate series of experiments, small pieces of calibration metals and certain binary alloys were placed close together and heated below their melting points; it was not possible to detect temperature differences in the various specimens and for this reason emissivity corrections were not applied to the equation above.

X-ray powder diffraction specimens were obtained by either filing or crushing the various alloys after they had been subjected to the isothermal heat treatments. The filings were sealed in quartz ampules and quenched in liquid argon from the temperature at which the corresponding solid sample had been heat treated.

REFERENCES

1. F. W. Clarke and H. S. Washington (1924), U. S. Geological Survey, Professional Paper 127. 117 pages.

2. "The Structure of Metals and Alloys," W. Hume-Rothery (1947), The Institute of Metals. Grosvenor Gardens, London. pp. 57-68.

3. B. T. Matthias, "Superconductivity in the Periodic System," Progress in Low Temperature Physics (1957) vol. II, pp. 136-150. Interscience Publishers Inc., New York.

4. H. J. Wallbaum, Naturwissenschaften (1943), 31, 91-92.

5. E. Raub, P. Walter, and M. Engel, Zeitschrift für Metallkunde (1952), 43, 112-118.

6. A. H. Geisler, and J. B. Newkirk, American Institute of Mining and Metallurgical Engineers (1948), 15, 1-20, Technical Publication 2444.

7. M. V. Cohen, Zeitschrift für Kristallography (1936), 94, 288-298.

8. M. V. Cohen, Zeitschrift für Kristallography (1936), 94, 306-310.

9. J. B. Nelson, and D. P. Riley, Proceedings of the Physical Society of London (1945), 57, 160-177.

10. International Tables for X-Ray Crystallography, volume 1, The International Union of Crystallography, Kynoch Press, Birmingham England (1952) p. xi.

11. Dana's Textbook of Mineralogy, E. S. Dana. Fourth Edition. Edited by W. E. Ford. John Wiley & Sons, Inc.

12. W. Zachariasen, Zeitschrift für Physikalische Chemie (1927), 128, 39-48.

13. A. J. Bradley, Zeitschrift für Kristallographie (1937), 96, 20-37.

14. G. Brauer and R. Rudolph, Zeitschrift für Anorganische und Allgemeine Chemie (1941), 248, 405-424.

15. H. J. Wallbaum, Zeitschrift für Metallkunde (1941), 33, 378-381.

16. D. Harker, Journal of Chemical Physics (1944), 12, 315-317.

17. E. Epremian and D. Harker, Transactions of AIME (1949), , 267-273.

18. F. H. Ellinger and W. P. Sykes, Trans. American Society for Metals (1940), 28, 619.

19. G. Grube and O. Winkler, Z. Elektrochem (1938), 44, 413-422 and 423-428.

20. R. P. Elliot and W. Rostoker, Transactions AIME (1953), 197, 1203-1204.

21. F. Laues and H. J. Wallbaum, Naturwissenschaften (1939), 27, 674-675.

22. P. Duwez and J. L. Taylor, Transactions AIME (1950), 188, 1173-1176.

23. T. V. Philip and P. A. Beck, Transactions AIME (1957), , 1269-1271.

24. H. Höne, Annalen der Physik (1933), 18, 625-655.

25. "The Optical Principles of the Diffraction of X-Rays," R. W. James (1950), G. Bell and Sons Ltd., London.

26. W. H. Bragg, Proceedings of the Physical Society of London (1921), 33, 222-224.

27. J. C. M. Brentano, Proceedings of the Physical Society of London (1925), 37, 184-193.

28. H. J. Wallbaum, Naturwissenschaften (1943), 31, 91-92.

29. S. Berger, Acta Chemica Scandinavica (1953), 7, 611-622.

30. A. Guinier, Annales de Physique (1939), 12, 161.

31. "X-Ray Crystallographic Technology," A. Guinier, Hilger and Watts Ltd., London, 1952.

32. F. Kirchner, Annalen der Physik (1922), 69, 59-80.

33. C. H. Johansson and J. O. Linde, Annalen der Physik (1925), 82, 449-478.

34. C. H. Schramm, P. Gordon, and A. R. Kaufmann, Transactions AIME (1950), 188, 195.